A Study on Oxygen Mass Transfer

The Role of Fermentation Products in Stirred Tank Reactors

MSc Thesis in Life Science & Technology

Liselot Wagenaar

Delft University of Technology

TU Delft

A Study on Oxygen Mass Transfer

The Role of Fermentation Products in Stirred Tank Reactors

by

Liselot Wagenaar
4686691

Master program:	Life Science and Technology
Department:	Biotechnology
Section:	Bioprocess Engineering
Project Duration:	March, 2024 - December, 2024
Defence:	December 16th 2024
Daily supervisor:	Rik Volger - PhD Bioprocess Engineering
Supervisor:	Cees Haringa - Assistent Professor Bioprocess Engineering
Thesis committee:	Adrie Straathof - Associate Professor Bioprocess Engineering
	Marcel Vieira Lara - Assistant Professor Industrial Microbiology

TU Delft

Abstract

The oxygen mass transfer coefficient, $k_L a$, is a critical parameter in bioprocess performance, influencing the design of stirred tank reactors. During a fermentation process, the behavior of bubbles and the $k_L a$ can be effected by various components present in the broth. This study investigates the effect of organic compounds (ethanol, glycerol and acetic acid), which are produced during a yeast fermentation process (*S. cerevisiae*). It is concluded that acetic acid appears to decrease the geometric mean bubble diameter, in aqueous solutions. As a surfactant, the acetic acid molecules accumulate in the gas-liquid interface, thereby inhibiting bubble coalescence. This leads to an increase in interfacial area and a 34% rise in $k_L a$ has been measured. Glycerol, however, showed no significant impact in water. Ethanol should exhibit a similar trend to acetic acid, as reported in previous literature (Puiman, Elisiário, et al., 2022). Remarkably, when these organic compounds were added to growth medium for a yeast fermentation - which consist of synthetic medium, glucose and vitamins - the effects were negligible. This likely due to the coalescence-enhancing properties of antifoam, which is present in synthetic media. On the other hand, the concentrations of the organic compounds tested were relatively low. In addition, during the fermentation process, the production of organic compounds did not significantly affect the bubble size. A slight increase in $k_L a$ was observed, arguably due to a reduction in working volume.

Whilst performing the tests, the $k_L a$ was measuring with three different experimental determination methods: the dynamic pressure method, the dynamic gassing-out method, and the gaseous oxygen balance method. The dynamic gassing-out method appeared a bit more consistent than the dynamic pressure method, possibly due to pressure stabilization issues. The gaseous oxygen balance method did not provide consistent results throughout the entire fermentation, as the method is sensitive and relies on very accurate gas measurements, especially when the oxygen consumption is low. The dynamic gassing-out method proved to be stable and provided the most results used for comparisons of experiment. However, considering its limitations, it requires validation with a ground truth, such as a validated reliable chemical method.

The experimental $k_L a$ data was compared with predicted values, using empirical correlations. All predicted values remained within 50% margin to the experimental values (determined with dynamic gassing-out method). To be able to use these prediction models in bioprocess design, further investigation is essential.

Acknowlegdements

During the course of this thesis, I received help and support from various individuals, and I am grateful to all who contributed to its completion.

First, I would like to thank my daily supervisor, Rik Volger. Your expertise gave me guidance throughout the project while still giving me space to explore my personal interests, such as yeast fermentations. Your broad understanding of the field often gave me the context I needed to move forward. I appreciated your willingness to support me, even during very busy periods. Thank you for your mentorship and constructive feedback!

I would also like to express my gratitude to Cees Haringa for his supervision during this project. Our meetings fostered interesting discussions and offered valuable insights that enriched my work. Additionally, thanks to my thesis committee members: Adrie Straathof and Marcel Vieira Lara.

Setting up the equipment and running an entire yeast fermentation process is no simple task. For this reason, I would like a special thanks to Christiaan Mooiman for you patience helping me set everything up and teaching me the essential lab techniques. Furthermore, I am grateful to Maarten Klaverdijk, who frequently assisted me when I encountered equipment challenges in the lab. Given that the batch processes were lengthy, I often had to be in the lab outside of regular office hours. I am thankful to Miki Segami and Rik Volger for spending an entire evening with me in the lab, and to Stef van Hateren, who supervised me when I needed to inoculate my reactor in the middle of the night. Stef, your enthusiasm, even when I attempted to revive a computer from the previous century in my search for specific equipment, did not go unnoticed. I also want to express my gratitude to the other technicians from BPE, Simon Leygeber and Jeroen Schmidt, for always being willing to help or share a small talk in the quiet of the empty lab. Finally, Dirk Geerts, your extensive experience often provided answers when everyone else seemed at a loss. Thank you for your support.

In my search for equipment to measure viscosity and surface tension, I am grateful to the Chemical Engineering department for guiding me and allowing me to use their devices. A special thanks to Christiaan Schinkel, Duco Bosma, Aleksandra Kondakova, and Anand Raja for their assistance and expertise.

Also, I would like to thank my office friends, for the nice coffee breaks and support when I needed it! Thanks to the CASE group, and the entire BPE group, for creating such a welcoming en engaging learning environment.

Finally, I wish to express my thankfulness to my friends and family. They supported me and listened to all my lab stories, even when the technical details likely made no sense to them. Your encouragement motivated me throughout this process.

I would like to acknowledge the use of OpenAI's ChatGPT during the preparation of this thesis. It has shown to be very helpful to improve clarity in writing, generating alternative phrasing and debugging LaTeX and python codes. All content generated with the aid of ChatGPT was critically reviewed and edited to ensure its accuracy and alignment with the academic standards of this work.

Nomenclature

Symbols

a	m^2/m^3	Interfacial area
A_b	m^2	Surface area of bubble
A_{ST}	m^2	Cross sectional area of stirred tank
c_L	mol/m^3	Liquid phase gas concentration
c_L^*	mol/m^3	Liquid phase gas concentration (saturated)
d_b	m	Bubble diameter
d_{32}	m	Sauter mean diameter
D	m^2/s	Diffusion coefficient
D_L	m^2/s	Diffusion coefficient of the gas in the liquid
D_R	m	Diameter of Rushton turbine impeller
D_{ST}	m	Diameter of Stirred Tank
F_{O_2}	mol/h	Flow of oxygen
g	m/s^2	Gravitational acceleration
H	$mol\ m^3/bar$	Henry's law constant
k	$Pa\ s^n$	Consistency index
k_c	$Pa\ s^n$	Casson consistency index
k_G	m/h	Gas phase mass transfer coefficient
k_L	m/h	Liquid phase mass transfer coefficient
k_La	h^{-1}	Volumetric mass transfer coefficient
n	-	Number of bubbles
n	-	Flow behavior index
N	s^{-1}	Rotation rate
OTR	$mol/s \cdot m^3$	Oxygen Transfer Rate
OUR	$mol/s \cdot m^3$	Oxygen Uptake Rate
p	bar	Pressure
p^o	bar	Partial pressure
P	$W = kg \cdot m^2/s^3$	Power
Po	-	Power number
P/V	W/m^3	Power to volume ratio
Q_G	m^3/s	Gas flow rate
r_b	m	Radius of bubble
r_{ST}	m	Radius of stirred tank
s	$1/s$	Surface renewal rate
t_e	s	Exposure time
U_s	m/s	Superficial gas velocity
V_b	m^3	Volume of a bubble
V_G	m^3	Volume of gas
V_L	m^3	Volume of liquid
V_{TOT}	m^3	Total volume
v	m/s	Velocity
y_{O_2}	-	Oxygen gas fraction

γ	s^{-1}	Shear strain rate
ϵ	-	Gas holdup
μ	h^{-1}	Growth rate
μ_c	$Pa\ s$	Casson viscosity
μ_{eff}	$Pa\ s$	Effective viscosity
μ_g	$Pa\ s$	Gas viscosity
ρ	kg/m^3	Density
σ	N/m	Surface tension
τ	Pa	Shear stress
τ_0	Pa	Shear yield stress

Dimensionless numbers

$$We = \frac{\rho \cdot v^2 \cdot d_b}{\sigma} \tag{1}$$

$$Re_{flow} = \frac{\rho \cdot d_b \cdot v}{\mu} \tag{2}$$

$$Re_{rotation} = \frac{\rho \cdot N \cdot D_R^2}{\mu} \tag{3}$$

$$Fr = \frac{D_R \cdot N^2}{g} \tag{4}$$

$$Po = \frac{P}{\rho \cdot N^3 \cdot D_R^5} \tag{5}$$

$$Sh = \frac{k_L \cdot d_b}{D} \tag{6}$$

$$Sc = \frac{v}{D} = \frac{\mu}{\rho \cdot D} \tag{7}$$

Contents

1 Introduction

1.1. Context of research project

Microbial fermentation is a powerful and sustainable tool in industrial biotechnology (Li et al., 2014). Industrial fermentation processes use various microorganisms to convert raw materials into industrial products, for example, biomass, chemical compounds, and proteins (Humphrey and Lee, 1992). The use of microorganisms in manufacturing processes is considered a more environmentally friendly alternative to traditional chemical and energy-intensive processes (Verma, 2022). In the field of bioprocessing, aerobic fermentation processing takes a prominent position, due to its shorter duration and increased process intensity compared to anaerobic fermentation (Verma, 2022).

An essential condition for aerobic fermentation is sufficient oxygen availability. Oxygen molecules must be dissolved in the fermentation broth to be accessible to the cells. However, oxygen is a very hydrophobic molecule, resulting in low solubility in water (Straathof and Heijnen, 2020), which causes a challenge for effective mass transfer. As a result, the oxygen mass transfer coefficient ($k_L a$) often becomes a limiting factor, especially when scaling up the process (Garcia-Ochoa and Gomez, 2009). For example, Vos et al. (2015) reported that they had to operate their aerobic cultures at reduced growth rates due to oxygen transfer constraints.

This thesis focuses on oxygen mass transfer, but the same trends are expected for other gases with low solubility in water, such as CO, CO_2 and H_2 (Puiman, Elisiário, et al., 2022). These gases are substrates in syngas fermentation, a process that uses gas molecules to produce value-added compounds, such as ethanol (Phillips et al., 2017). When renewable syngas is used, this technology may contribute to sustainable chemical production in a circular, biobased manner (Elisiário et al., 2022). Nevertheless, just like in aerobic fermentation, gas-liquid mass transfer limits the fermentation rate, particularly in the case of a high cell density process (Abubackar et al., 2011).

In literature, it is shown that the oxygen mass transfer rate could be affected by various factors, such as operating conditions (Muregi et al., 2021) and and broth composition (Volger et al., 2024). Franz et al. (1980) also noted that organic solutes impact gas holdup and bubble size, both of which are linked to mass transfer. During a fermentation process, different organic compounds are produced, affecting bubbles and mass transfer dynamics (Zieminski and Hill, 1962). For example, in fermentations with baker's yeast, *S. cerevisiae*, the most abundant product is ethanol, plus a minor amount of other by-products such as acetate and glycerol (Otterstedt et al., 2004). Even in the presence of oxygen, yeast cells can metabolize glucose by alcohol fermentation, instead of fully oxidizing glucose to water and CO_2 (Busti et al., 2010). This capacity makes yeast an interesting model system. When the concentrations of these products rise throughout the batch process, it could be hypothesized that their effect on bubbles also increases. Therefore, this thesis examines how these fermentation products influence gas bubble behavior and the oxygen mass transfer.

In this thesis, oxygen mass transfer is the central focus, quantified by the overall oxygen transfer coefficient ($k_L a$). The $k_L a$ is an important scale-up factor and often used to compare the efficiency of bioreactors (Moutafchieva et al., 2013). The a in $k_L a$ represents the interfacial area: the area available

for mass transfer. Since the interfacial area is directly related to bubble size, gas bubble sizes were measured in various solutions in a stirred tank reactor. Additionally, the $k_L a$ was determined using three experimental methods: the dynamic gassing-out method, the dynamic pressure method, and the gaseous oxygen balance method, to evaluate which method is the most feasible.
This thesis also examines the effects of organic compounds produced during a yeast fermentation process, specifically acetic acid, ethanol, and glycerol. These compounds were studied in water-based systems and their effects were also obtained in a fermentation process. Since fermentation broths contain numerous other components, their potential influence on $k_L a$ is also considered.
The $k_L a$ measurements were compared with predictions from empirical correlations. These correlations required the measurement of liquid properties, such as surface tension and viscosity, which were obtained from the fermentation samples. The rationale for the chosen research direction and the research questions are provided in Section 1.4.

1.2. Theoretical background

1.2.1. Oxygen Mass Transfer

The Oxygen Transfer Rate (OTR) is the amount of oxygen transferred from the gas to the liquid phase (Straathof and Heijnen, 2020). In a fermentation process, the rate of oxygen consumption by the microorganisms is defined as the Oxygen Uptake Rate (OUR) (Garcia-Ochoa et al., 2010). The uptake rate capacity exceeds the oxygen transfer capacity, and therefore the OTR equals the OUR. The OTR (Equation 8) is determined by the driving force ($c_L^* - c_L$) and the volumetric mass transfer coefficient ($k_L a$). The driving force is the difference between the maximum dissolved oxygen concentration (c_L*, solubility), which can be determined with Henry's law (Equation 9, Phillips et al., 2017), and the actual dissolved oxygen concentration c_L.

The parameter $k_L a$ is often treated as a single entity in mass transfer studies, but it is also interesting to study k_L and a separately. The term k_L, representing the liquid-side mass transfer coefficient, will be discussed in section 1.2.2. The interfacial area, a is directly linked to the diameter of the gas bubbles, as smaller bubbles have a relatively larger area for mass transfer (Equation 13, Heijnen and Van't Riet, 1984). Additionally, the interfacial area a is also related to the gas holdup via Equation 10. The gas holdup (Equation 11, Lehrer, 1971) is defined as the volume fraction of gas within the total volume (gas and liquid phases combined) (Tao et al., 2019). The superficial gas velocity (Equation 12) is the velocity at which gas passes upwards through a stirred tank (Saravanan et al., 2009). As many of these parameters and equations are related, an overview of these relationships is shown in Figure 1.1.

$$OTR = k_L a \cdot (c_L^* - c_L) \tag{8}$$

$$c_L^* = H \cdot y_{O_2} \cdot p \tag{9}$$

$$a = \frac{6 * \epsilon}{d_{32}} \tag{10}$$

$$\epsilon = \frac{V_G}{V_G + V_L} \tag{11}$$

$$U_s = \frac{Q_G}{A_{ST}} = \frac{Q_G}{\pi \cdot r_{ST}^2} \tag{12}$$

$$a = \frac{n \cdot A_b}{V_L} = \frac{n \cdot 4\pi r_b^2}{V_L} \tag{13}$$

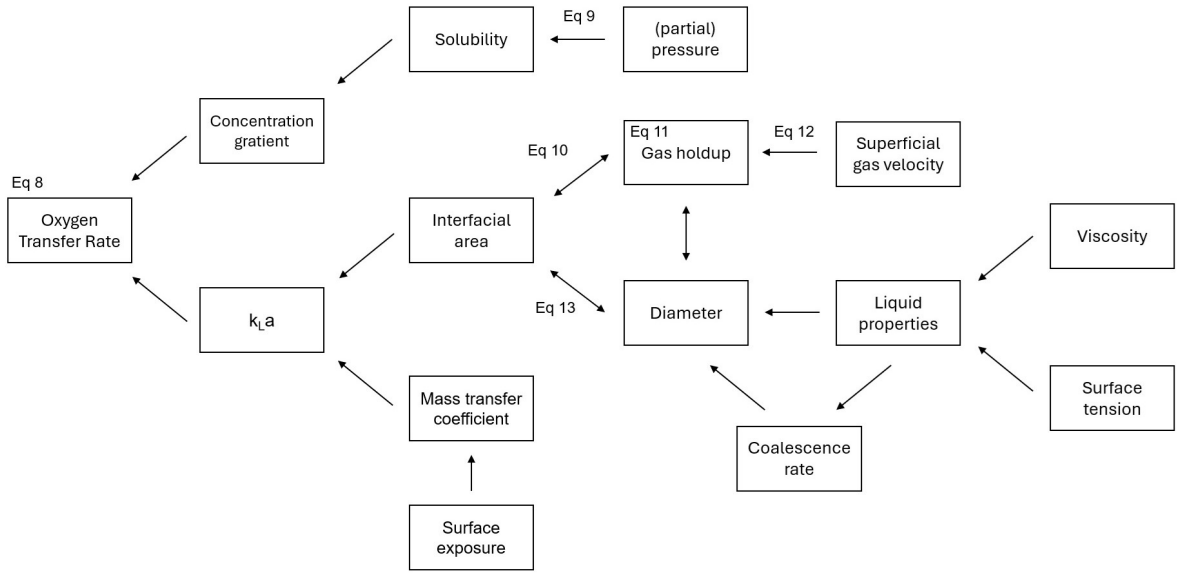

Figure 1.1: Interrelated parameters with effect on the oxygen mass transfer in a stirred tank reactor.

1.2.2. Mass transfer description models

This section delves into the mass transfer coefficient, k_L, by exameing it through mass transfer models. As the k_L is affected by many conditions, such as broth composition, temperature and bubble diameter (Straathof and Heijnen, 2020), a deeper understanding of these models provides valuable insights into how these conditions impact mass transfer.

Two film model

When oxygen is introduced into the system through air bubbles, mass transfer occurs from the gas phase to the liquid phase. This can be described by the film model, a theory invented by Nernst in 1904 and later developed by Lewis and Whitman (1924) into the two film model (Sherwood, 1974). When considering an air bubble in water, the oxygen concentrations in the gas is higher than in the liquid, which drives diffusion of molecules across the interface. Each phase is well mixed, but turbulence dies out at the phase boundary (Doran, 2013), where equilibrium is achieved between the two phases. Between the interface and the bulk, the model assumes two stagnant films, where a concentration gradient exists, shown in Figure 1.2. Oxygen molecules will diffuse from the gas bulk into the gas film, then from the gas film into the liquid film, and finally into the liquid bulk.

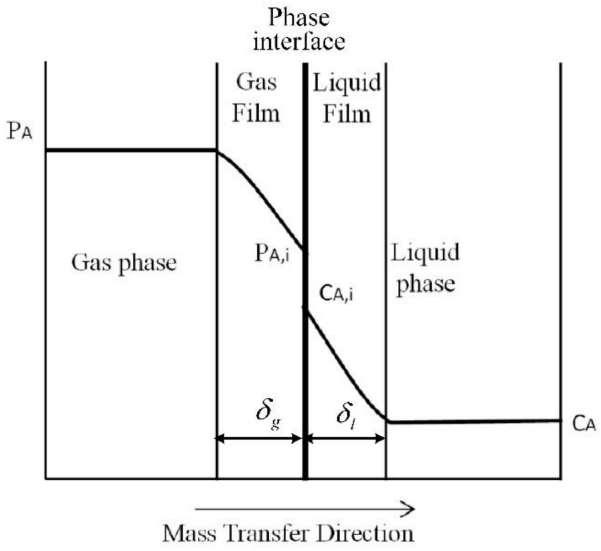

Figure 1.2: Stagnant film at the gas-liquid interface around a gas bubble, described by two film theory (Wen et al., 2021).

The theory assumes that all resistance to mass transfer relies in the films, rather than the bulk liquid (Mishra and Upadhyay, 2022). Both films have their own resistance, represented by the gas-phase and liquid-phase mass transfer coefficients, k_G and k_L, respectively. As the oxygen diffusion in the gas phase is much faster than in the liquid phase, the mass transfer resistance of the gas film is negligible (Heijnen and Van't Riet, 1984), and only the parameter k_L is obtained to determine the mass transfer.

Penetration theory

The two film model assumes hypothetical stagnant films, but the velocity at the surface is not truly zero (Treybal, 1955). According to Perlmutter (1961), this simplification does not adequately capture the complexities of mass transfer mechanisms between phases. Higbie (1935) stated that the time of exposure between the phases is short, so that the concentration gradient would not have time to develop (Treybal, 1955). To replace the two film theory, Higbie proposed the penetration theory. This model describes the liquid phase as being composed of "packages" (Chung, 1968), shown in Figure 1.3. As a gas bubble rises in the liquid, the liquid packages slip along the bubble's surface, where they are

exposed to the gas for a finite period before being replaced. During this period of exposure, diffusion of oxygen molecules occurs, and the change in concentration penetrations into the small package. It is assumed that each of the packages stays in contact with the gas for the same period of time (NPTEL, 2013).

The mass transfer coefficient can be calculated with Equation 14 (Garcia-Ochoa and Gomez, 2005). The value of k_L depends on the molecular diffusion coefficient, D, and the exposure time t_e.

$$k_L = 2 \cdot \sqrt{\frac{D}{\pi \cdot t_e}} \tag{14}$$

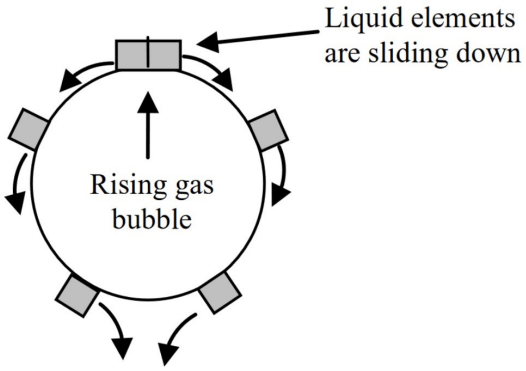

Figure 1.3: Higbie's penetration theory (NPTEL, 2013)

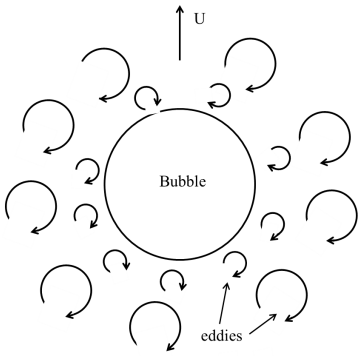

Figure 1.4: Danckwerts' surface renewal theory (Liao and Lucas, 2018)

Surface renewal theory

The penetration theory has a significant assumption that the contact time for all the packages is the same. While this may be plausible in laminar flows, it is often unrealistic in most real-world scenarios (Mishra and Upadhyay, 2022). In an effort to apply Higbie's approach in turbulent systems, Danckwerts (1951) assumed that the bubble surface is periodically refreshed by eddies, which are rotating fluid regions (Figure 1.4. These eddies continuously expose fresh liquid to the gas, while sweeping away and mixing parts of the surface which have been in contact with the gas back into the bulk. Eddies are exposed for various lengths of time (Treybal, 1955), and during the time of exposure the liquid absorbs gas.

Within this theory, k_L can be determined with the diffusion coefficient and the surface renewal rate, s, which represents the same volume of liquid that is being renewed (Morsi and Basha, 2015).

$$k_L = \sqrt{D \cdot s} \tag{15}$$

1.2.3. Bubble flow & behavior

This section explores bubble dynamics and behavior, which play a key role in determining bubble size. Understanding these mechanisms is essential for describing the effect of organic solutes and other fermentation broth components.

Flow pattern

In order to understand the oxygen mass transfer, it is essential to examine the hydrodynamic phenomena within the bioreactor. In gas-liquid stirred tank reactors, operation flow regimes are broadly classified into three categories: the flooding regime, loading regime, and the complete dispersion regime (Shewale and Pandit, 2020 & Warmoeskerken and Smith, 1985). In the complete dispersion regime, gas bubbles recirculate continuously both above and below the impeller, causing gas to be distributed uniformly throughout the vessel. The bioreactor system in this study operates within the complete dispersion regime, characterized by turbulent flow that includes vortex formation and substantial mixing within the reactor. According to Doran (2013), Rushton turbines generate a radial flow pattern, creating separate circulation currents both above and below each impeller. Visual observation of the flow patterns were compared with those documented by Hoseini et al. (2021) and Taghavi et al. (2011), and the patterns are illustrated in Figure 1.5.

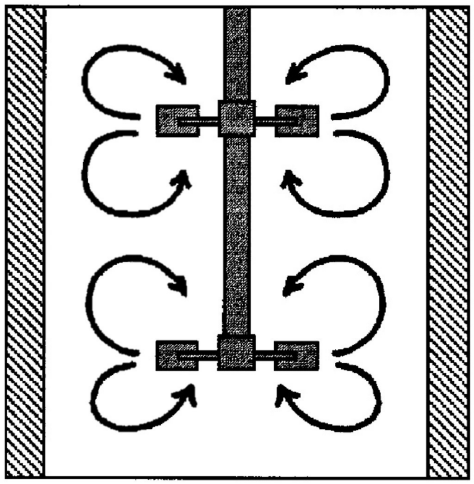

Figure 1.5: Flow pattern in stirred vessel equipped with dual Rushton turbines (Rutherford et al., 1996).

Bubble formation and break-up

In aerated stirred tank reactors, gas is introduced through the sparger, generating bubbles at the submerged orifices (Martín et al., 2008a). Next, the impeller rotation moves these initial bubble into the blades, where they break-up due to collision with the blades and are subsequently dispersed at the discharge stream (Martín et al., 2008b). According to Shimizu et al. (1999), the bubble break-up can also result from strong shear forces present in the boundary layer of the impeller blade.

Beyond break-up at the impeller, bubbles can also break within high kinetic energy turbulent eddies (Hasan, 2017). Nambiar et al. (1990) stated that breakage is likely to occur in the zone surrounding the impeller, where the turbulence intensity is very high. Hinze (1955) described the break-up via bulgy deformation due to turbulent flow. Local pressure differences cause initial bulges on the surface of the globule, which develop into protuberances, leading to the bubble splitting up. This mechanism can also be described as a balance between disruptive forces acting on a bubble and stabilizing surface tension forces (Alves et al., 2002). When the ratio of the two forces exceeds a critical value, the bubble breaks.

Bubble coalescence

When two (or more) bubbles in a liquid come into contact and merge to form a single, larger bubble, this is called bubble coalescence (Figure 1.6). Coalescence can occur when two bubbles collide, trapping a small amount of liquid between them, known as the dimple. Subsequently, this liquid drains until the liquid film separating the bubbles reaches a critical thickness (Prince and Blanch, 1990). At this point, the intermolecular forces between the bubbles become prominent, leading to a rupture of the film and causing the bubbles to merge together (Zieminski et al., 1967). If the time period is not sufficient for the film to reach its critical thickness, the bubbles do not coalesce.

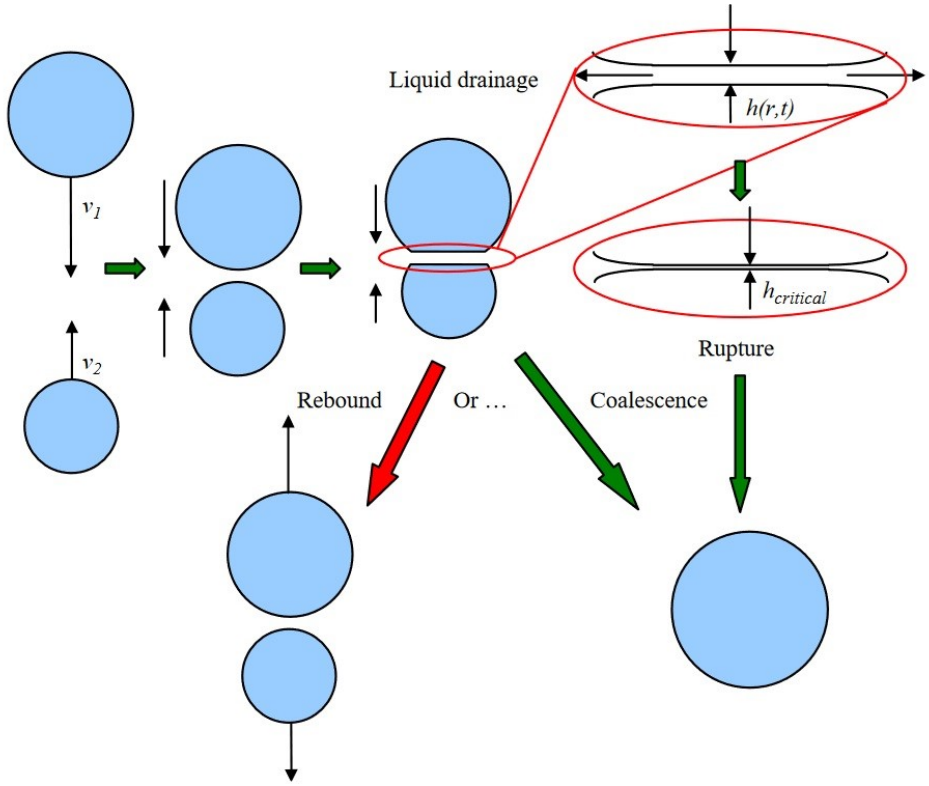

Figure 1.6: Bubble coalescence mechanism (P. Chen et al., 2005)

1.2.4. Effects of organic solutes

Adding organic compounds to the system alters key liquid properties, such as surface tension and viscosity. These properties also change during the progression of a fermentation process (Garcia-Ochoa and Gomez, 2005), for example by the production of alcohols and acids. These changes significantly impact bubble dynamics and thereby also the bubble size, leading to variation in $k_L a$. Therefore, it is valuable to study how organic solutes influence the hydrodynamic processes described in Section 1.2.2 and 1.2.3. Other components commonly found in fermentation broths are also evaluated.

Organic solute molecules have an amphiphilic structure, comprising a hydrophilic (polar) group and a hydrophobic (apolar) segment, typically a hydrocarbon chain. These molecules are surface active, meaning they tend to accumulate in the gas-liquid interface (Keitel and Onken, 1982). The hydrophilic group will point into the liquid phase, forming hydrogen bonds with water molecules, while the hydrophobic part aligns with the gas phase. By interfering with and thereby disrupting the strong hydrogen bonds between water molecules, these solutes weaken surface cohesion, reducing the surface tension.
As the carbon chain length of organic molecule increases, the overall polarity of the compound decreases (Jamialahmadi and Müller-Steinhagen, 1992). Formic acid, which is highly polar, readily blends with the water molecules. In contrast, acetic acid, with a more hydrophobic carbon chain, integrates less into the water phase, and will accumulate in the gas-liquid interface. Therefore, this effect becomes more pronounced with compounds possessing longer carbon chains.

Effects on bubble behavior

Regarding bubble formation at the orifices, Alves et al. (2002) suggest that surfactants do not have a significant effect on the initial bubble formation process. Bubble break-up, however, is influenced by the density, viscosity and interfacial tension of the two phases (Hinze, 1955). The extent of deformation is effected by the stabilizing interfacial tension and deforming forces of turbulent eddies (Nachtigall et al., 2012). If the stabilizing interfacial tension decreases, the breakage rate will increase (Bąk and Podgórska, 2013), which will decrease the bubble diameter (Sathyagal et al., 1996). Nambiar et al. (1990) also indicated that surfactants promote bubble break-up though reduction of the interfacial tension. Their mechanism proposes that pressure fluctuations not only induce surface depressions, but also remove surfactant molecules at the interface. As a results, the freshly generated dynamic interfacial tension in that region is higher than the static interfacial tension on the rest of the bubble, which generates an inward flow. This additional stress promotes this breaking mechanism, as illustrated in Figure 1.7.

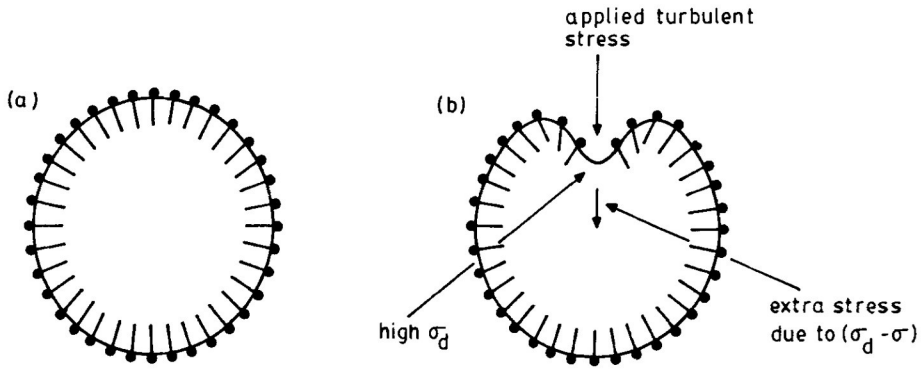

Figure 1.7: Bubble break-up mechanism influenced by surfantant molecules (Nambiar et al., 1990).
(a) Bubble before interaction with eddy (b) Formation of bulge .

Just like the bubble break-up process, coalescence is also affected by solutes. According to Heijnen and Van't Riet (1984), the coalescence rate is dependent on the liquid surface properties, varying

from coalescing (e.g. pure liquids) to non-coalescing (e.g. water-salt systems). Alves et al. (2002) confirmed that the bubble diameter is larger in coalescing systems than in non-coalescing systems. In non-coalescing systems, merging of bubbles can be hindered by surfactants via coalescence inhibition, described by Keitel and Onken (1982). This mechanism involves the hydrophilic group in the liquid phase. The oxygen atoms in the polar group are more electronegative and will draw electron density towards themselves, resulting in a partial negative charge, known as surface polarization. Therefore, repulsive forces arise between two closely approaching bubbles, thereby inhibiting the first step of bubble coalescence, illustrated by the red arrow in Figure 1.6.
The inhibition of bubble coalescence can also be described by the Marangoni-effect. Due to nonuniform surfactant distributions along the gas-liquid interface, a surface tension gradient arises (Taghavi et al., 2011). This induces Marangoni flow towards the center on the dimple (Lu et al., 2019), slowing the drainage of the film, and thereby inhibiting bubble coalescence. Another recognized effect is that when a bubble rises through the liquid, the Marangoni stress rigidifies the bubble interface. This increases the drag force, thereby decreasing the bubble rising velocity (Wang et al., 2024).

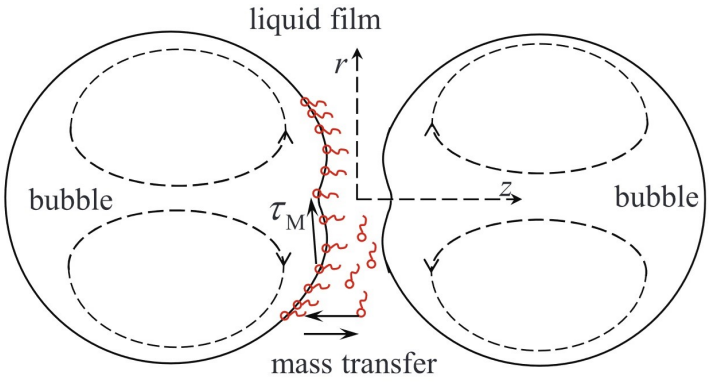

Figure 1.8: Bubble coalescence inhibition by the Marangoni-effect. The Marangoni stress (τ_M) induced inwards flow, preventing film drainage (Wang et al., 2024).

Although this thesis focuses on organic compounds, it is important to consider other components present in fermentation broths. One of the key components of synthetic media is salts, with the detailed composition provided in Table 2.1. According to Heijnen and Van't Riet (1984), the addition of salts makes a liquid non-coalescing. Considering the coalescence mechanism in Figure 1.6, Arjunwadkar et al. (1998) explained that the presence of electrolytes causes a surface tension gradient in the film between the two interacting bubbles, known as the Gibbs-Marangoni pressure (Rommens, 2024). This gradient suppresses film thinning, preventing the bubbles form merging together. Coalescence inhibition becomes significant when the salt concentration exceeds the transition concentration. This transition concentration makes the point at which the bubble size shifts from its initial size (uninfluenced by salt) to its final size (affected by salt).
Duignan (2021) provided a more extensive explanation of this process. He stated that when certain mixtures of surface-enhancing and surface-depleting salts are used, their effects can counterbalance each other, resulting in no inhibition of coalescence.

The occurrence of foam in bioprocesses is very common and the generally adopted strategy to control it is the use of an antifoam agent (Arjunwadkar et al., 1998). Antifoam agents tend to enhance the bubble coalescence, resulting in larger bubble sizes (Kawase and Moo-Young, 1990) and a reduction of interfacial area.

In addition to the surface tension, liquid viscosity is also a property that can impact bubble behavior. According to Heijnen and Van't Riet (1984), high viscosity results in larger bubbles in a bubble column. Similarly, Arjunwadkar et al. (1998) observed an increase in the proportion of large bubbles due to

enhanced coalescence. This is further supported by Pedersen et al. (1994), who reported that higher viscosity promotes bubble coalescence.

Effects on mass transfer models

When surfactants accumulate at the gas-liquid interface, shown in Figure 1.2, they can influence the mass transfer coefficient k_L. Garcia-Ochoa and Gomez (2005) state that the surfactants will form a mono-layer, inhibiting oxygen diffusion and introducing additional resistance to the mass transfer. This phenomenon is confirmed by Dai et al. (2004), who note that the molecules reduce the mass transfer efficiency by hindering the oxygen transport through the interface. This accumulation occurs with organic solutes, such as alcohols and acids, as well as antifoam agents (McClure et al., 2017) and proteins (Arjunwadkar et al., 1998), all of which create an additional barrier to oxygen transfer at the gas-liquid interface.

Observing the mass transfer models described in Figure 1.3 and 1.4, the presence of surface-active agents can alter the surface properties of bubbles. According to J. Vasconcelos et al. (2003), the accumulation of these molecules will change the bubble from being mobile to rigid. Bubbles with mobile surfaces will contain more curvature, while rigid bubbles tend to behave like solid spheres. Baird and Davidson (1962) explains that the surface-active molecules suppress the formation of ripples, reducing disturbances at the gas-liquid interface. J. Vasconcelos et al. (2003) emphasizes that Higbie's penetration theory (Figure 1.3) applies only to bubbles with mobile surfaces. The mobility of the surface determines the rate at which new liquid is brought into contact with the gas, which influences the gas transfer rates (Prins and Van'T Riet, 1987). Therefore, a rigid interface will lead to a reduction in the liquid film mass transfer coefficient k_L (McClure et al., 2017).

Besides, Haycock and Garner (1959) point out that contamination with surface active agents decreases circulation. Smaller bubbles are related with a smaller degree of turbulence (Pedersen et al., 1994). Heijnen and Van't Riet (1984) demonstrated a relation between the reduction in k_L and the reduction in bubble size (for bubbles smaller than 2 mm), as smaller bubbles have less circulation. According to Khan (1990), if the surface is contaminated, than the frequency of surface renewal - in which eddies are impelled into the interface - must be damped, leading to a reduction in mass transfer coefficient k_L.

The viscosity of the continuous phase also impacts the mass transfer coefficient. An increase in viscosity reduces the degree of liquid turbulence (García-Ochoa and Gómez, 1998). Diminishes turbulent eddies will lead to less surface renewal (Volger et al., 2024), thereby decreasing the mass transfer. In a fermentation broth, high concentrations of biomass are expected to influence the broth viscosity and thus the k_L (Puiman, Elisiário, et al., 2022). Glucose is often used as carbon source and also increase the viscosity of the solutions (Rivas-Interián et al., 2019).

1.2.5. Experimental $k_L a$ determination

Numerous experimental methods to determine the $k_L a$ are described in literature. Chemical methods, such as the sulfite oxidation method or the CO_2 absorption method, are unsuitable for microbial processes (Garcia-Ochoa and Gomez, 2010) and were therefore not used in this project. Instead, physical and biological methods, which can be applied in the presence of living cells, are described below.

Dynamic gassing-out method

This method is one of the most extensively described methods in literature. In this approach, oxygen is first removed from the solution by sparging it with nitrogen. Afterwards, air is reintroduced, and the dissolved oxygen (DO) profile is monitored using a DO probe (Van't Riet, 1979). The mass balance for the dissolved oxygen concentration is shown in Equation 16. By integrating this, the equations in Figure 1.9 are derived.

$$\frac{dc_L}{dt} = k_L a \cdot (c_L^* - c_L) \tag{16}$$

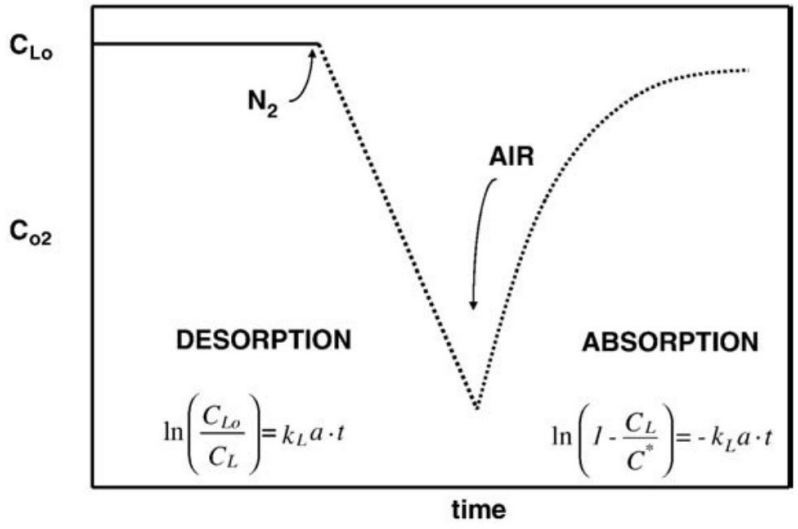

Figure 1.9: Dissolved Oxygen profile during dynamic gassing-out method (Garcia-Ochoa and Gomez, 2009)

Unfortunately, this method has some limitations. The DO probe has a certain response time, causing a delay in the measurements. According to Van't Riet (1979), the response time is defined as the time needed to record 63% of a stepwise change. For this project, the response time was determined to be 17 seconds (determination is provided in Appendix C), suggesting that a correction would improve accuracy. Nonetheless, due to time constrains, implementing this correction is outside the scope of this project.

Furthermore, this method assumes that the gas phase is ideally mixed, a condition that is not met in these experiments. According to Linek et al. (1991), this is a severe limitation, causing erroneous $k_L a$ values. During the bubbles' residence in the solution, oxygen transfer to the liquid phase alters the gas composition, resulting in a non-uniform mixing across bubbles. Additionally, the transition from nitrogen (N_2) to air does not instantaneously replace the gas within bubbles. The non-coalescing nature of the fermentation broth further hinders bubble merging, preventing uniform gas composition.
It is worth mentioning that the lack of ideal gas phase mixing is more pronounced at large-scale bioreactors, as highlighted by Linek et al. (1989). Studies using this method often apply it on larger scales;

for instance, Chang et al. (1989) uses a 38 L bioreactor and Dang et al. (1977) a 50 L bioreactor. Given that the bioreactor in this study is only 1.5 L, the impact of non-ideal gas mixing is expected to be less significant. For a 1.5 L bioreactor, the transition period between two gases was estimated to be approximately 4 seconds. In significantly larger bioreactors, this transition period is expected to be considerably longer.

Dynamic pressure method

This method is proposed by Linek et al. (1989), as an alternative to the dynamic gassing-out method. Instead of changing the gas composition, a pressure step is introduced, which causes a simultaneous change in oxygen concentration across all bubbles of the dispersion. As shown in Equation 9, the maximum dissolved oxygen concentration can be adjusted by either modifying the oxygen composition (y_{O_2}) or the pressure (P). Scargiali et al. (2010) later proposed a simplified dynamic pressure method, which significantly reduces data processing complexity. This simplified approach yields a similar data treatment to the dynamic gassing-out method, as both share the same underlying principle.

Gaseous oxygen balance method

The third method relies on the oxygen mass balance in the gas phase. This approach assumes uniform distribution of oxygen concentration in both the gas and liquid phase, resulting from ideal mixing. Another key assumption is steady-state conditions, resulting in the following gas-phase oxygen mass balance:

$$\frac{dN_{O_2}}{dt} = F_{O_2}^{in} - F_{O_2}^{out} - V_L \cdot OUR = 0 \tag{17}$$

The oxygen consumption by the cells (OUR) is equal to the Oxygen Transfer Rate, which is shown in Equation 8. By rearranging the equation, the $k_L a$ can be calculated.

$$k_L a = \frac{F_{O_2}^{in} - F_{O_2}^{out}}{V_L \cdot (c_L^* - c_L)} \tag{18}$$

1.2.6. Bubble size measurements

Bubble sizes are measured in various systems using different methods. Many researchers use cameras to capture bubble images, either with a photo-optical probe submerged in the solution (Puiman, Elisiário, et al., 2022) or with a high speed photographic camera (Basařová et al., 2018). Another approach involved guiding bubbles through a glass capillary and measuring their diameter with a photoelectric probe (Keitel and Onken, 1982). In this thesis, a conical optical fiber is employed for bubble measurements, referred to as the fiber probe.

The probe is put into the solution pointing downwards and performs measurements on the bubbles that get pierced by the tip. The measurement relies on the reflection of a laser beam at the tip of the probe. A laser signal is emitted through the probe, where it gets partially reflected at the tip, and the internal refraction is then detected by an optoelectronic module (A2 Photonic Sensors, 2019). The refraction in air is at least a tenfold higher than in water, allowing the phase at the fiber tip to be determined (Lefebvre et al., 2022). By distinguishing these two phases, the void fraction (gas holdup) is easily obtained by measuring the time fraction when the probe is submerged in air (A2 Photonic Sensors, 2019). The laser refraction is illustrated in Figure 1.10.

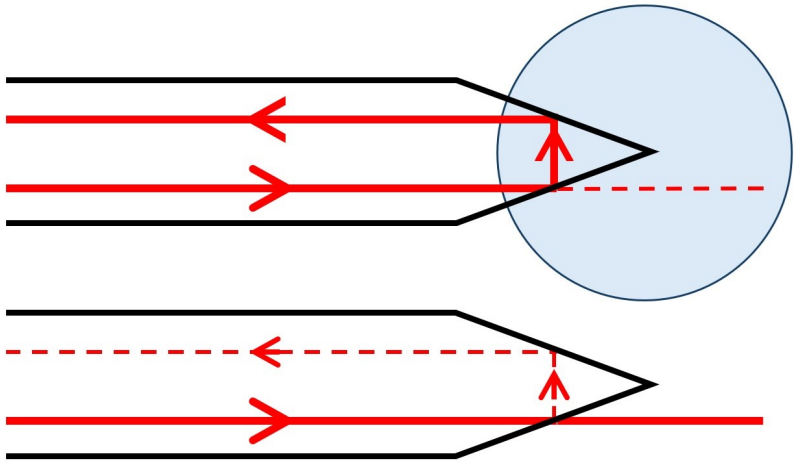

Figure 1.10: Internal refraction of the fiber probe. The laser refraction is higher when the probe's tip is submerged in gas (above) than in liquid (below)

Figure 1.11 shows the measurement of a single bubble, with increased voltage when the fiber tip is immersed in the gas phase. In addition to the residence time, the exit velocity of each bubble is measured to determine its size. This velocity is derived from the measured Doppler signal, combining the wave reflected at the fibers tip and at the G/L interface (Lefebvre et al., 2022). With both the velocity and the residence time of the individual bubble, the bubble size can be determined. If both the entry and exit velocity cannot be measured properly, the corresponding bubble is considered invalid.

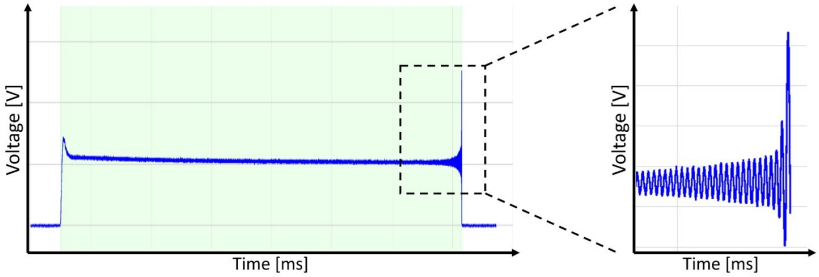

Figure 1.11: Measurement profile of a valid bubble (Rommens, 2024). The oscillation is enlarged to improve the readability.

1.2.7. Empirical $k_L a$ correlations

To predict $k_L a$ values, a high number of correlations are proposed in literature, in both dimensional and dimensionless form (Garcia-Ochoa and Gomez, 2010). These correlations are functions of many factors that influence the $k_L a$, such as the geometry of the vessel and stirrer, physico-chemical properties of liquids, the superficial gas velocity and the operational conditions (Gagnon et al., 1998 and García-Ochoa and Gómez, 1998).

Correlations with exponential variables

Van't Riet (1979) proposed a relation for the determination of the $k_L a$ in stirred vessels for non-viscous systems (Equation 19). Many authors applied linear regression on their data with this equation, resulting in a wide variation of exponent values. The variables α and β generally have values between 0 and 1 (Calderbank and Chandrasekharan, 1981).

$$k_L a = C \cdot U_s^{\alpha} \cdot \left(\frac{P}{V}\right)^{\beta} \tag{19}$$

As the $k_L a$ is also correlated with the liquid effective viscosity, García-Ochoa and Gómez (1998) included that parameter, obtaining Equation 20. The constant C depends on the geometrical parameters of the vessel and stirred employed, and the exponent values again show a great variation among authors (Gagnon et al., 1998). García-Ochoa and Gómez (1998) also proposed to substitute P/V by the stirred speed N, as can be seen in Equation 21.

$$k_L a = C \cdot U_s^{\alpha} \cdot \left(\frac{P}{V}\right)^{\beta} \cdot \mu_{eff}^{\gamma} \tag{20}$$

$$k_L a = C \cdot U_s^{\alpha} \cdot N^{\beta} \cdot \mu_{eff}^{\gamma} \tag{21}$$

These correlations will be affected by the rheological model used to describe the effective viscosity, as the fermentation broth is a non-Newtonian fluid. The rheological models are elaborated on in Appendix J.

Dimensionless correlations

Besides the dimensional relations above, literature also proposes many dimensionless correlations, including more parameters than the previous ones.

García-Ochoa and Gómez (1998) proposed the correlation shown in Equation 22. The authors describe the viscosity with the Ostwald-de Waele model, also known as the power law model.

$$k_L a = 9.8 \cdot \left(\frac{\rho N^{2-n} D_R^2}{k K^{n-1}}\right)^{2/3} \cdot \left(\frac{N D_R}{U_S}\right)^{-2/3} \cdot \left(\frac{\rho N^2 D_R^3}{\sigma}\right) \cdot \left(\frac{D_L}{D_R^2}\right) \tag{22}$$

García-Ochoa and Gómez (1998) proposed another correlation (Equation 23), in which they used the Casson model to describe the viscosity.

$$k_L a = 0.3 \cdot \left(\frac{\rho N D_R^2}{\mu_c}\right) \cdot \left(\frac{N D_R}{U_s}\right)^{-2/3} \cdot \left(\frac{\rho N^2 D_R^3}{\sigma}\right) \cdot \left(\frac{D_L}{D_R^2}\right) \tag{23}$$

Perez and Sandall (1974) proposed another correlation (Equation 24). They also assumed that the

relationship between shear stress and shear rates can be represented by the power law. However, they adjusted the calculation of the effective viscosity, as can be found in Appendix J.

$$k_L a = 21.24 \cdot Re_{rotation}^{1.11} \cdot Sc^{0.5} \cdot \left(\frac{D_R U_s}{\sigma}\right)^{0.447} \left(\frac{\mu_g}{\mu_{eff}}\right)^{0.694} \cdot \left(\frac{D_L}{D_R^2}\right) \tag{24}$$

Finding correlations that align with the experimental conditions in this thesis proved to be challenging. Therefore, it must be notes that the equations proposed by García-Ochoa and Gómez (1998) were originally developed for stirred vessels equipped with two six-curved-blade turbines, rather than the six flat-blade turbines (Rushton) used in this study. Furthermore, Equation 24 was designed for systems with a single six flat-blade turbine, whereas two turbines were used in the conducted experiments for this thesis.

1.3. Literature

This section outlines the relevant findings from literature on the studied organic compound, specifically acetic acid, ethanol, and glycerol. The effects of these compounds are examined in both water-based systems and fermentation broths. In fermentation processes, the potential influence of other components should also be considered.

Effect of organic compounds in water systems

Numerous studies have investigated the effects of organic solutes on bubble sizes and oxygen mass transfer in water-compound solutions. For instance, Zieminski and Hill (1962) demonstrated that the rate of oxygen transfer from air bubbles to water increases when small quantities of specific alcohols or carboxylic acids are added to the solution. Additionally, Zieminski et al. (1967), reported a threefold increase in bubble surface area and a 4.5-fold increase in oxygen mass transfer rate specifically due to acetic acid. Jamialahmadi and Müller-Steinhagen (1992) found that alcohols (including ethanol) and organic acids (including acetic acid) reduce bubble size, leading to a higher gas holdup. They observed a 38% reduction in bubble diameter due to ethanol and a 45% reduction due to acetic acid. Additionally, Keitel and Onken (1982) determined for many organic compounds an inhibition concentration for coalescence restraint, where bubble size significantly decreased. These thresholds were 20 mM for ethanol, and 0.2 mM for acetic acid. Studies on the effect of glycerol on bubble sizes have primarily focused on very high concentrations, ranging from 27% to 100% (Franz et al., 1980, Samaras et al., 2014), far exceeding the concentration levels found in fermentation broths (Table 3.2). This is likely to investigate the effect of viscosity, rather than bubble coalescence inhibition. Özbek and Gayik (2001) studied the $k_L a$ in glycerol solution and found no change in its value between 0% and 10% glycerol.

Effect of ethanol in fermentation broths

Puiman, Elisiário, et al. (2022) demonstrated a 74% reduction in Sauter diameter in ethanol solution, resulting in a sixfold increase in $k_L a$. Similar trends, albeit to a lesser extent, were observed in medium and fermentation broths. Although a decrease in k_L was observed, the significant increase in interfacial area more than compensated for this, resulting in enhanced oxygen mass transfer. Puiman, Abrahamson, et al. (2022) also simulated gas-liquid mass transfer in an industrial CO-to-ethanol fermentation process and observed an increase in mass transfer coefficient. They attributed this to ethanol production inhibiting bubble coalescence, resulting in smaller bubbles. Beyond these two studies by Puiman, literature on the influence of organic fermentation products - such as glycerol and acetic acid - on mass transfer in fermentation broths remains scarce. One notable finding in the literature is from Braasch and Braasch (1934), who observed that adding 0.01% to yeast wort reduced bubble size and thus increased the transfer area. However, the details of this patent are not publicly accessible.

Effect of other fermentation broth components

It is also valuable to consider what is known in literature about other fermentation components. The batch fermentation begins with glucose, vitamins, and synthetic medium, which contains among others salts and antifoam (Pluronic PE6100). Further details about the additives are provided in Table 2.1. Arjunwadkar et al. (1998) demonstrated that the addition of salts makes liquids non-coalescing, exhibiting higher mass transfer rates. Specificly, the effect of $(NH_4)_2SO_4$ was examined by Rommens (2024), who reported a transition concentration beyond which coalescence is inhibited. The concentration in our medium exceeds this proposed threshold. Additionally, Rivas-Interián et al. (2019) studied medium contraining KH_2PO_4 $MgSO_4$, showing an increase in interfacial area and $k_L a$, attributed to the inhibition of bubble coalescence.

Arjunwadkar et al. (1998) reported a substantial decrease in mass transfer coefficient at increasing antifoam concentration, although their study uses a different antifoam component than the one present

in our medium. Additionally, other authors demonstrated even that low concentrations of antifoam agents can reduce oxygen mass transfer (McClure et al., 2017; Morão et al., 1999; J. Vasconcelos et al., 2003). Similarly, Elibol (1999) observed a significant reduction in $k_L a$ caused by Pluronic F-68, a compound similar to Pluronic PE6100, though differences in physical properties may result in varying effects.

Regarding glucose, Garcia-Ochoa and Gomez (2005) reported a 11% decrease in $k_L a$ with the addition of 10 g/L. In contrast, Rivas-Interián et al. (2019) reported a minimal decrease in bubble diameter and minimal increase in $k_L a$. These findings suggest that the reported results are inconclusive, although the overall impact of glucose appears to be relatively low.

As biomass is produced during the fermentation process, the cells may also have effect. Puiman, Elisiário, et al. (2022) stated that high biomass concentrations (10 g/L) are expected to influence the broth viscosity and thus the k_L. In contrary, some authors propose that cells enhance oxygen mass transfer by consuming oxygen as it diffuses through the gas-liquid interface ((Garcia-Ochoa & Gomez, 2005; Tsao, 1968)).

Experimental $k_L a$ determination methods

The three methods used in this thesis for $k_L a$ determination have been reviewed literature by various authors. The dynamic gassing-out method is considered simple and relatively accurate (Garcia-Ochoa et al., 2010). However, several authors have highlighted that response time of the dissolved oxygen (DO) probe can lead to inaccuracies in $k_L a$ determination (Cerri et al., 2016, Tribe et al., 1995). Additionally, Linek et al. (1991) demonstrated that that this method tends to underestimate $k_L a$ values due to limitations in gas phase mixing.
The dynamic pressure method has been shown to produce accurate $k_L a$ values, as reported by Linek et al. (1989). This approach was further validated in a simplified form by Scargiali et al. (2010), confirming its reliability.
According to Van't Riet (1979), the gaseous oxygen balance method offer a straightforward $k_L a$ determination. However, it requires high gas flow rates and highly sensitive measuring equipment (Garcia-Ochoa and Gomez, 2009). Cruz et al. (1999) reported inadequate results with this method, explained by the low rate of oxygen consumption by the microorganism.

Empirical $k_L a$ correlations

Considerable efforts have been made to establish quantitative relationships for $k_L a$ in terms of associated variables (Rivas-Interián et al., 2019). Numerous authors have proposed correlations based on their experimental oxygen mass transfer data. For instance, Van't Riet (1979) developed a correlation for water systems that depends on the power-to-volume ratio and the superficial gas velocity, achieving an accuracy of 20-40 %. Supported by Equation 19, he illustrated a relationship between $k_L a$ and P/V, suggesting that increased stirring power consumption or reduced volume would lead to a higher $k_L a$. Building on this, Gagnon et al. (1998) created correlations for various impeller geometries, which provided a sufficiently accurate representation of their experimental data.
For more complex systems, such as non-Newtonian fluids, García-Ochoa and Gómez (1998) proposed a dimensionless correlation that expressed the Sherwood number as a function of the Reynolds and the Weber number, with a reported error of ± 10%. Additionally, Perez and Sandall (1974) fitted experimental data to a comparable correlation with a standard deviation of 5%.

1.4. Research gap & Project scope

Given that the $k_L a$ can be influenced by a large variety of settings, geometries and solutes, various fermentation conditions were considered when choosing the direction of this research. During the setup of this research it was ensured that the variable factors, proposed to be studied, should be applicable on a yeast fermentation process.

Experimental settings
The impeller speed was set at 400 rpm, as higher speeds made it impossible to measure bubble sizes with the fiber probe. Investigating the effects of different sparger types could provide valuable insights; however, precise observation would require measuring bubble diameters directly at the sparger (Heijnen and Van't Riet, 1984). This is challenging because the fiber probe is fixed in permanent positions within the ceiling of the bioreactor. Additionally, since yeast cells grow optimally at 30°C, the temperature was fixed at this level.

Fermentation broth components
During a fermentation process, proteins are excreted by the cells. According to S. Chen et al. (1992), air bubble diameter decreases with increasing protein concentration, but the available data is limited. Besides, regulating protein concentration during fermentation is challenging, as cells naturally excrete proteins. Data about the effect of biomass is also limited, but the literature indicates that cells have a small effect on coalescence rate (Volger et al., 2024). Regulating biomass concentration is equally difficult, and it cannot be isolated from other variables during fermentation, making it challenging to observe the effects.
Sugars such as glucose and sucrose are commonly used as carbon sources in bioprocesses. In the batch fermentation processes conducted for this research, regulating sugar concentration is also challenging due to the nature of batch operations.
Excessive foam formation is undesirable from an operational perspective, making the addition of antifoams generally necessary to prevent foaming (Doran, 2013). Several studies indicate that low concentrations of antifoam agents can reduce oxygen transfer rates, as discussed in Section 1.3. Since the aim of this research is to enhance mass transfer, this will not primarily be the focus. However, it is important to note that antifoam agents are present in the synthetic media used in this study. The synthetic media also contains salts, and the presence of electrolytes is known to inhibit bubble coalescence, potentially enhancing mass transfer. However, salts can also act as inhibitors of *S. cerevisiae* (Casey et al., 2013) leading to reduced growth and ethanol yield (Wei et al., 1982).
Organic compounds, such as alcohols, carboxylic acids, glycols and ketones, are among the most prominent fermentation products. Keitel and Onken (1982) described their ability to decrease bubble size, making them relevant for further investigation. The first conducted fermentation revealed acetic acid, ethanol, and glycerol as the most abundant products. Consequently, this research focuses on these three compounds.

1.4.1. Research questions

Previous studies have demonstrated a clear relationship between organic compound concentrations and bubble sizes, enhancing oxygen mass transfer, as described in Section 1.3. However, most experiments were conducted in water system, excluding the influence of other fermentation broth components. To address this gap, this research includes measurements performed throughout yeast fermentation processes, and the following research question was established:

1. What is the effect of fermentation products (acetic acid, ethanol, and glycerol) on the interfacial area of gas bubbles, and therefore also the oxygen mass transfer ($k_L a$) in a stirred tank reactor?

The $k_L a$ can de determined experimentally using various methods. Previous literature describes certain

inaccuracies and limitations associated with the three methods obtained in this research. These uncertainties, along with interest in the practical implementations of the methods, lead to the formulation of the second research question.

2. What is the most feasible experimental method to determine the oxygen mass transfer ($k_L a$) in a stirred tank reactor?

With the growing interest in the design of bioprocesses, like fermentations, understanding the most influential parameters is essential for accurate $k_L a$ prediction (Puiman, Elisiário, et al., 2022). Many correlations to predict the $k_L a$ are proposed in literature, leading to the third research question.

3. Is it possible to predict the oxygen mass transfer ($k_L a$) in a stirred tank reactor with empirical correlations within an acceptable deviation range?

2
Materials & Methods

2.1. General setup & devices

The experiments were conducted with an 1.5 L bioreactor from Applikon Biotechnology, integrated with a Biostat B Plus benchtop bioreactor controller from Sartorius. The bioreactor was equipped with two 6-blade Rushton turbine impellers, which were rotated at 400 rpm by the Stirrer Controller P100 from Applikon Biotechnology. Each impeller has a diameter of 4.5 cm and a blade height of 1.15 cm and they were positioned 5 cm apart along the central shaft. The temperature was maintained at 30 °C throughout the experiments. For the abiotic measurements, the volume was 1 L. The gas flow rate was set at 0.5 L/min, with a gas composition of 30% air and 70% nitrogen gas. This was equal to an oxygen feed flow of 78 mmol/h, creating an oxygen-limited environment during fermentation. The yeast strain used in these experiments was *Saccharomyces cerevisiae* (CEN.PK.113-7D). An initial volume of 1.4 L was required to account for the volume reduction as samples were withdrawn from the fermentation broth. A detailed description of the medium composition and fermentation additives, including glucose and vitamins, is provided in Table 2.1. All experimental conditions, including those for the abiotic tests, were selected to mimic actual fermentation conditions.

Component	Formula	Product Code	Concentration
Ammonium Sulphate	$(NH_4)_2SO_4$	Merck 1211	5 g/L
Potassium dihydrogen phosphate	KH_2PO_4	Merck 4877	3 g/L
Magnesium sulphate.7H_2O	$MgSO_4 \cdot 7H_2O$	Baker 0168	0.5 g/L
Pluronic PE6100		BASF 50073570	0.2 g/L
Trace elements - Appendix A		Stock solution	1 mL/L
D(+)-Glucose Monohydrate	$C_6H_{12}O_6 \cdot H_2O$	J.T.Baker 0113	28 g/L
Vitamins - Appendix A			1 mL/L

Table 2.1: Composition of synthetic media for *S. cerevisiae* (row 1-5) and other added nutrients (row 6-7) (de Hulster, 2019a). Details about the Trace elements and vitamins are provided in Appendix A

The dissolved oxygen concentration was measured with a Dissolved Oxygen (DO) probe (PM10/794) from AppliSens Sensor Innovation. The solution was sparged with a gas mixture (30% air, 70% nitrogen gas) to calibrate the 100% level of dissolved oxygen. The gas composition of the off-gas was measured with the ServoPro 4900 Multiga from Servomex. The inflowing gas was controlled with two Smart Mass Flow Controllers from Brooks. All data was logged with the computer using MFCS Shell Software. To apply pressure on the bioreactor, a pressure head from Tescom Europe.

The biomass concentration during the fermentation was determined with Optical Density (OD) measurements at a wavelength of 660 nm, conducted with Spectrophotometer UV-1800 from Shimadzu. Additionally, 10 mL fermentation broth was filtered to remove the liquid, and dried on the filter in the microwave. Following, he dry weight was determined with a laboratory scale to quantify the biomass. The

concentrations of other compounds, like sugars and acids, were measured using High Performance Liquid Chromatography, model 1260 Infinity from Aligent Technologies.

The viscosity measurement were performed using a DHR-3 Rheometer from TA Instruments, equipped with the Concentric Cylinder geometry. The device brought the sample up to 30 °C, consistent with the temperature used in all experiments. During the measurement, shear stress (± 1 Pa) was applied, and the resulting shear strain rate was measured. From this data, the effective viscosity was determined using different rheological models, explained in Appendix J.

The surface tension measurements were conducted with a Bubble Pressure Tensiometer (BPT Mobile, KRÜSS Scientific). Since these measurements were performed at 20.5 °, a temperature correction was applied. Following the methodology outlined by Perez and Sandall (1974), the correction was assumed to be the equivalent to that which applies to the surface tension of water against air (Janssen and Warmoeskerken, 1987).

The density was determined by weighing 1 mL of the sample. The volume was collected using a 1 mL Pipetman from Gilson, and its weight was measured with the AG204 DeltaRange balance from Mettler Toledo. Preferable, a density meter from Anton Paar was used for these measurements, but that device is not suitable for samples that contain cells.

The velocity and size of individual bubbles were measured with the M2 Analyzer from A2 Photonic Sensors. The acquisition frequency was 15625 kHz (estimated maximum velocity 1.2 m/s), pretrigger was 100 μs and block duration was 30.000 or 40.000 μs. The exposed length of the optical fiber is ± 7.1 mm, with a diameter of 125 μm, a microscopic picture is shown in Figure 2.1. The probe was positioned in the solution pointing downwards, measuring the diameter of bubbles pierced by the fiber. A detailed description of the operation principle of the device is provided in Section 1.2.6. After the measurement, a bubble size distribution was generated from all valid bubbles. Further data processing is described in Appendix D.
According to van der Bom (2023), ± 1000 valid events are required for an accurate determination of the bubble size, which was challenging to achieve in this setup. Bubbles are measured properly if they approach the probe from below, which is often disrupted in turbulent flow. The optimal position of the probe tip, yielding the highest validation rate, was determined to be 15 cm above the workbench. This corresponds to 1 cm above the highest Rushton turbine, and the flow at this position moves upwards (Figure 1.5).
The bubble sizes measured by the fiber probe were validated using pictures captured with the Sony Alpha A7 II camera. Details of the verification are provided in Appendix B.

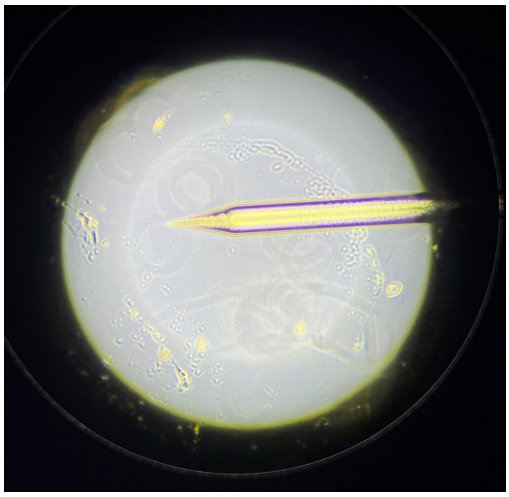

Figure 2.1: Fiber probe tip observed under a microscope

2.2. Experimental $k_L a$ determination

Three different methods were deployed to determine the $k_L a$ in various conditions. They are described more profoundly in Section 1.2.5.

Dynamic gassing-out method

This method is based on a step-change in the inlet gas oxygen concentration. The solution was first sparged with nitrogen and then with the 30% air / 70% N_2 mixture, to create an absorption profile, comparable to the one shown in Figure 1.9. The $k_L a$ value was obtained from the absorption profile, by fitting the curve to the data using the `scipy.curve_fit` function in Python.

Dynamic pressure method

In addition to the dynamic gassing-out method, the dynamic pressure method was employed. Instead of introducing a step change in oxygen concentration, a step change in pressure was applied. However, increasing the pressure from 1 to 1.2 bar required up to 2 minutes, which was too long compared to the actual measurement duration. To address this, the pressure was released instead, creating a desorption profile, comparable to the one in Figure 1.9. Following the same approach as the dynamic gassing-out method, the $k_L a$ values were determined by curve fitting.

Gaseous oxygen balance method

The third method was based on the gaseous oxygen mass balance, and the $k_L a$ could be determined with Equation 18. The OTR was determined by measuring the oxygen concentration in the inflowing and outflowing gas, while c_L was measured with a DO probe (Van't Riet, 1979). The saturation concentration, c_L^*, was calculated using Henry's law (Equation 9), in which the outlet gas concentration is used for y_{O_2} (Garcia-Ochoa and Gomez, 2010).

Since this technique is based on precise oxygen concentration measurements, highly sensitive measuring equipment is essential (Garcia-Ochoa and Gomez, 2009). Especially if the oxygen uptake is low, the concentration difference between the inlet and outlet gas stream is minimal. To enhance accuracy, additional controls and measurements have been implemented. The inlet oxygen concentration was monitored continuously throughout the fermentation, rather than being assumed constant at 20.95%. The mass flow controllers were validated, and if required, flow adjustments were made. The atmospheric pressure in the laboratory was also monitored, instead of assuming that it is always exactly 1 atm. The reactor volume is accurately determined by weighing samples and marking the bioreactor for consistent volume reference. Additionally, the bioreactor seals are verified to prevent any gas leaks. As the temperature in the lab was 20.5°C, this value was used for ideal gas law calculations.

2.3. Conducted experiments

To investigate the effect of fermentation broth components on the bubble size and $k_L a$, the abiotic experiments outlined in Table 2.2 were conducted. The focus was on three organic compounds: acetic acid, ethanol, and glycerol, as these were the most abundant products from the fermentations. The tested concentration range for these organic compounds was based on their levels in the final fermentation sample (Table 3.2). Due to time constrains, ethanol could not be tested individually. However, its effects on the bubble size and $k_L a$ have been previously studied in a stirred tank reactor (Wagenaar, 2021, Puiman, Elisiário, et al., 2022).

A yeast batch fermentation process requires nutrients, thus glucose, vitamins and synthetic media must be present. To assess the effect of fermentation products, the impact of these additives was also studied.

Medium	**Additives**	**Concentration**
Water	Acetic acid	0 - 5 mM
Water	Glycerol	0 - 20 mM
Synthetic medium	-	-
Synthetic medium	Glucose Vitamins	28 g/L 1 mL/L
Synthetic medium	Glucose Vitamins Ethanol Glycerol Acetic acid	28 g/L 1 mL/L 120 mM 20 mM 5 mM

Table 2.2: Overview of conducted abiotic experiments.

Three batch fermentations were performed with the medium composition provided in Table 2.1. On September 19th, 8.3 mM acetic acid was added to the broth at the start of the fermentation, to observe its potential effects during a fermentation process. All fermentations were intentionally oxygen limited (30% air, 70% N_2), to examine whether improvement by acetic acid would be possible.

	Date	**Additives**
Ref1	August 28th	-
Aa1	September 19th	8.3 mM acetic acid
Ref2	October 22nd Unit 1	-
Ref3	October 22nd Unit 2	-

Table 2.3: Caption

2.4. Empirical $k_L a$ correlations

Besides experimental determination of the $k_L a$, it is interesting to compare the obtained values with values from prediction models, described in Section 1.2.7. The conditions that were used in the performed experiments, and the measured liquid properties of the fermentation samples are used as input for the correlations. The constants and exponential variables were retrieved from literature, to compare the values proposed by different authors.

Equation 19 is designed for water systems, and therefore used to predict $k_L a$ values that are compared with experimental $k_L a$ values from experiments with water. For the mixtures with organic compounds, due to low concentrations, the effects on liquid properties were minimal, leaving it outside of the scope of this thesis. To predict the $k_L a$ during the fermentation processes, correlations with exponential variables (Equation 20 and 21) en dimensionless correlations (Equation 22, 23, and 24) were applied. The experimental conditions are shown in Table 2.4, and the measured liquid properties are presented in the Results, Section 3.3.

Parameter			**Reference**
Diffusion coefficient	D_L	$2.5 \cdot 10^{-9}\ m^2/s$	Xing et al., 2014
Diameter of impeller	D_R	$4.5\ cm$	
Rotation rate	N	$6.67\ s^{-1}$	
Power	P	$0.295\ W$	Equation 5
Power number	Po	5.4	Janssen and Warmoeskerken, 1987
Power to volume ratio	P/V	$295\ W/m^3$	
Superficial gas velocity	U_s	$1.061 \cdot 10^{-3}\ m/s$	Equation 12
Volume	V	$1 \cdot 10^{-3}\ m^3$	
Gas viscosity	μ_g	$20.63 \cdot 10^{-6}\ Pa\ s$	Lemmon and Jacobsen, 2004
Density	ρ	$995.68\ kg/m^3$	Janssen and Warmoeskerken, 1987

Table 2.4: Parameters used for empirical $k_L a$ correlations. The table also includes parameter to calculate the power with Equation 5.

3
Results & Discussion

3.1. Abiotic experiments

3.1.1. Dynamic $k_L a$ determination methods

Two similar dynamic methods were used to experimentally determine the $k_L a$: the dynamic pressure method and the dynamic gassing-out method. The conditions for this particular experiment were an exception compared to those described in Section 2.1, with a gas composition of 100% air a temperature maintained at 20.5 °C. The solution in the bioreactor was pure water.

	Pressure $k_L a$ (h^{-1})	**Gassing-out** $k_L a$ (h^{-1})
	51.56	40.93
	45.16	40.53
	48.83	42.29
	52.54	
Average	**49.52**	**41.25**
Standard deviation	2.86	0.75

Table 3.1: Experimental $k_L a$ values for two similar determination methods.

The results in Table F.1 show a difference in average $k_L a$ values obtained using the two dynamic methods. The standard deviation of the dynamic pressure method is a higher than that of the dynamic gassing-out method, reflecting greater variability among its measurements. This could be attributed to the available equipment, which required reading the pressure meter by eye and and manually adjusting the pressure. This made it challenging to achieve exactly 1.2 bar. However, the standard deviation is within an acceptable range, allowing the method to be applied in abiotic experiments with acetic acid.

3.1.2. Solutions with fermentation broth components

Before analyzing the bubble size data, it is important to note that these measurements do not represent the bubble sizes throughout the entire reactor. As Takahashi and Nienow (1993) demonstrated, bubble sizes can vary depending on their position within the reactor. Additionally, the fiber probe measures the bubble at the height where it pierces the bubble, which may not be exactly at the bubble's center.

Organic compounds

To study the effect of fermentation products on the bubble size and the k_La in a batch process, the impact of two individual organic compounds were tested: acetic acid and glycerol.

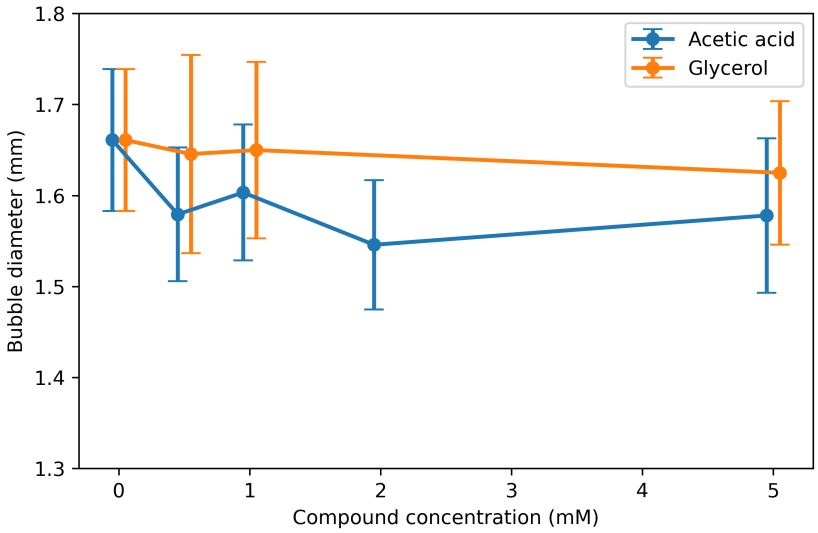

Figure 3.1: Geometric mean bubble diameter in water-compounds solutions in a stirred tank reactor. The error bars indicate the 95% confidence interval.

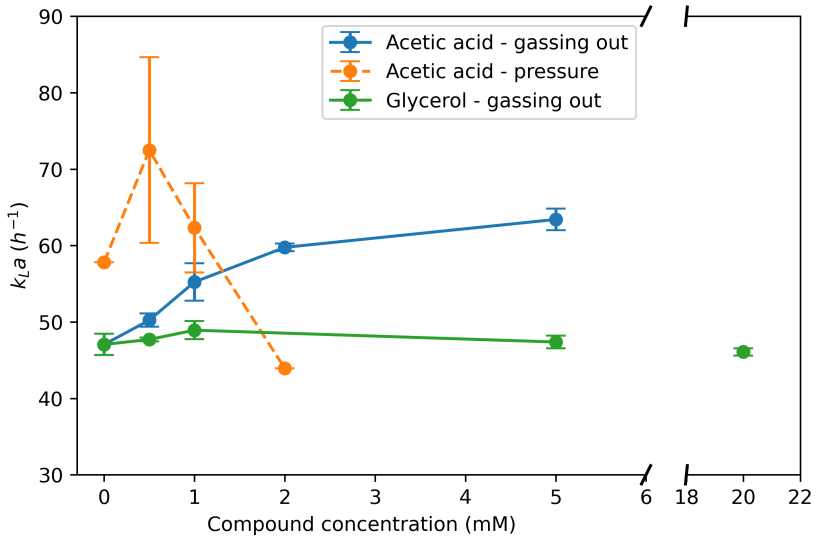

Figure 3.2: k_La results in water-compound solutions in a stirred tank reactor. The error bars indicate the standard deviation. All dynamic gassing-out measurements were performed in triplicate. For the dynamic pressure measurements a detailed explanation is provided in Appendix F.

In Figure 3.1 is shown that an increasing acetic acid concentration results in a reduction in bubble diameter of 7%. As a surfactant, acetic acid promotes bubble breakup through the mechanism illustrated in Figure 1.7 and inhibits bubble coalescence due to surface polarization. Both effects contribute to smaller bubbles, resulting in a larger interfacial area. Figure 3.2 demonstrates that as the bubble size in acetic acid solutions decreases, the $k_L a$ increases. The acetic acid molecules in the gas-liquid interface are assumed to hinder oxygen transport (Section 1.2.4). Additionally, as the gas bubbles become more rigid and less mobile, surface renewal is reduced, limiting transport. Despite the proposed reduction in k_L, the effect of increased surface area dominates, resulting in an overall increase in the mass transfer coefficient of 35% (Figure 3.2). These results for acetic acid align with the trends reported by Zieminski et al., 1967. However, the differences they observed were significantly larger, which might be due to the use of higher concentrations in their experiments.

Although ethanol was not individually examined in this thesis, literature (Wagenaar, 2021, Puiman, Elisiário, et al., 2022) suggests that its effects in aqueous solutions are similar to those of acetic acid, as discussed above.

On the other hand, within the tested concentration range, glycerol appears to have no significant effect on the bubble size (Figure 3.1) or the $k_L a$ (Figure 3.2), as the value remains relatively constant. This observation is consistent with the findings of Özbek and Gayik (2001), who reported no change in $k_L a$ a at low glycerol concentrations.

In Figure 3.2, the blue and green $k_L a$ values were determined using the dynamic gassing-out method. For acetic acid solutions, the dynamic pressure method was also applied. However, the results exhibit significant variability, as indicated by the relatively large error bars, and the $k_L a$ values do not align with those obtained from the dynamic gassing-out method. This deviation is likely attributed to the sensitivity of the DO probe, because the data points available for curve fitting were limited (elaborated in Appendix F). Consequently, these results do not provide additional insights into the dynamic pressure method. In practice, establishing a constant pressure of 1.2 bar before each $k_L a$ measurement proved time-consuming. The available pressure head required manual adjustment using a knob, followed by waiting for the pressure to stabilize before further adjustments could be made to reach the desired level. A more efficient approach would involve a device capable of setting a specific pressure level and automatically increasing the pressure until the target value is achieved.

Fermentation nutrients

The effect of fermentation additives, such as synthetic media and nutrients (Table 2.1), on bubble behavior and $k_L a$ was studies.

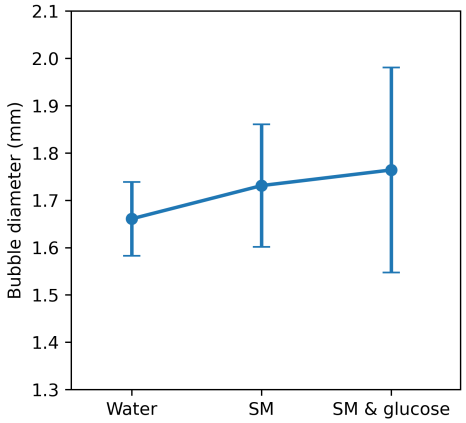

Figure 3.3: Geometric mean bubble diameter in water; synthetic media; synthetic media, glucose and vitamins. The precise composition is provided in Table 2.2.

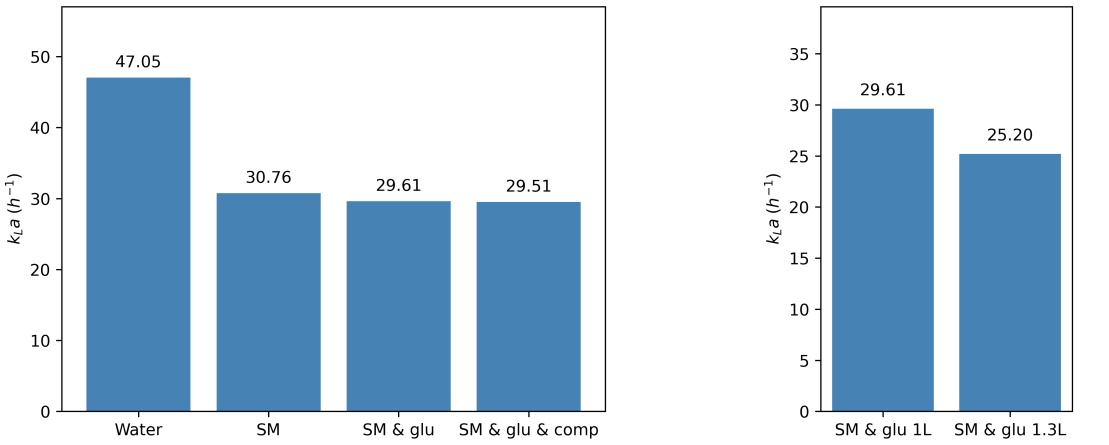

(a) Dynamic $k_L a$ values for different solutions.

(b) Dynamic $k_L a$ values for different volumes.

Figure 3.4: Comparison of dynamic $k_L a$ values for fermentation additives.
(a) From left to right compounds were added to the solution: water; synthetic medium; addition: glucose & vitamins; addition: acetic acid, ethanol, and glycerol. The compositions are detailed in Table 2.2.
(b) Solution with synthetic medium, glucose, and vitamins was tested at different volumes.

The bubble diameter in synthetic media was higher compared to water, and the addition of glucose caused a slight increase (Figure 3.3). However, the bubble data in this experiment is limited, resulting in large error bars. Despite this, the $k_L a$ results correlate with the bubble data, showing lower values for synthetic media and synthetic media with glucose (Figure 3.4a).
The fermentation additives in Table 2.1 can be obtained to analyse this result. Synthetic media includes salts, which are known to inhibit bubble coalescence, leading to smaller bubbles (Arjunwadkar et al., 1998). However, since the bubbles diameter increased compared to water (Figure 3.4a), the presence of Pluronic PE6100, the antifoaming agent, appears to have a stronger effect. Literature on the effect of this particular compound on bubble sizes is limited, but the decrease in $k_L a$ is in line with previous studies (Elibol, 1999, McClure et al., 2017). The addition of glucose to the synthetic medium causes a slight increase in bubble diameter and a corresponding decrease in $k_L a$. This could be attributed to a higher viscosity, reduced surface renewal, and a lower k_L (Volger et al., 2024). However, this remains speculative, and especially the small difference could be within the confidence interval.

The addition of organic compounds (to the solution with synthetic media and glucose) shows no significant impact on the $k_L a$ (Figure 3.4a). These findings suggest that while $k_L a$ could be increased in water-based experiments, the effect is negligible in the presence of synthetic media. However, it should be noted that the concentrations of organic compounds in these experiments were relatively low, corresponding to levels produced during oxygen-limited fermentations. For comparison, Puiman, Elisiário, et al. (2022) reported a remarkable change in $k_L a$ after the addition of 50 g/L ethanol, whereas only 5.5 g/L was added in this study.

Lastly, the effect of working volume was also observed, with solutions containing synthetic media, glucose and vitamins. Figure 3.4b demonstrates that $k_L a$ decreases at a higher working volume. In this experiment, the determination of $k_L a$ was based on the time required to reach 100% dissolved oxygen. Therefore, this results seems reasonable, as larger volumes require more time to saturate the water with oxygen. The results can be further explained by Equation 19, which indicates that a increase in volume leads to a lower P/V ratio, and consequently, a smaller $k_L a$.

3.2. Fermentations

Fermentation performance

To study bubbles size and k_La in yeast fermentation, three batch processes were successfully conducted. Approximately every hour, a sample was collected to measure the biomass and solute concentrations in the fermentation broth. Additionally, the dissolved oxygen was measured using a DO probe, and the CO_2 production was measured in the off-gas.

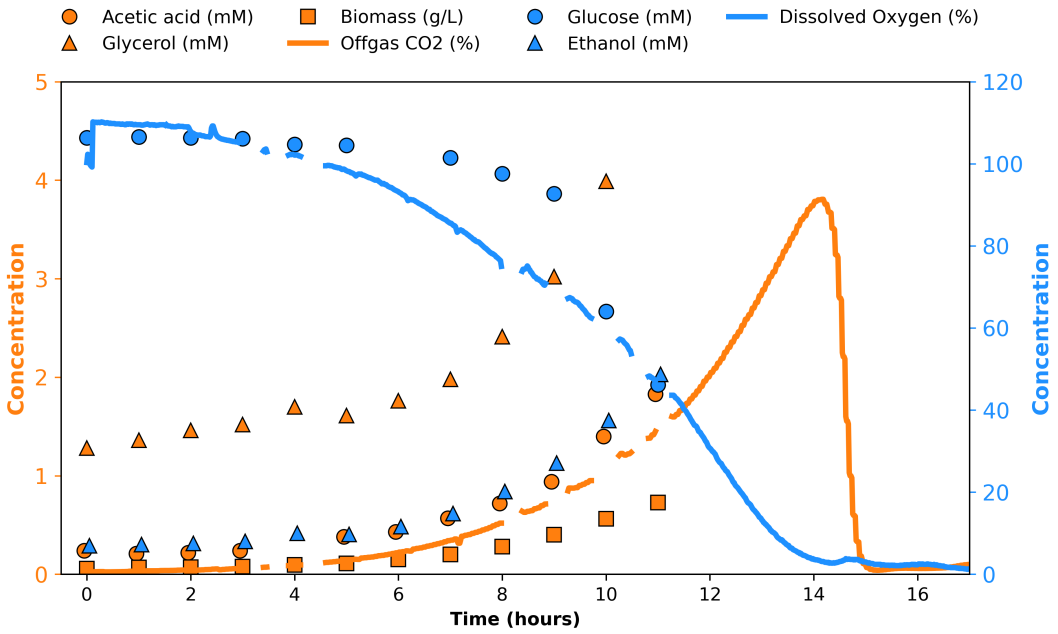

Figure 3.5: Concentrations of fermentation broth components and gas fractions throughout batch fermentation Ref1. The orange data corresponds to the left y-axis, and the blue data corresponds to the right y-axis. Fluctuations in the DO and off-gas CO_2 curves caused by dynamic gassing-out measurements were removed for improved readability.

Figure 3.5 shows the progress of fermentation Ref1. During fermentation, glucose and dissolved oxygen levels decreased, accompanied by an increase in biomass and the production of CO_2 and organic compounds (acetic acid, ethanol, glycerol). Progress data of Aa1, Ref2, and Ref3 are presented in Appendix G. Since the process takes approximately 15 hours, it was challenging to sample throughout the entire fermentation. For batches Ref1, Ref2, and Ref3, fermentation was initiated in the morning, leading to missing the final samples. On the contrary, batch Aa1 was inoculated late in the evening and progressed overnight, thus only the final stages were sampled.

Compound	Ref1	Aa1	Ref2	Ref3
Biomass	2.48 g/L	2.14 g/L	2.67 g/L	2.26 g/L
Ethanol	135 mM	134 mM	124 mM	119 mM
Glycerol	15.9 mM	19.3 mM	14.6 mM	11.9 mM
Acetic acid	2.37 mM	11.73 mM	4.26 mM	2.26 mM
Growth rate	0.07 h^{-1}	0.14 h^{-1}	0.12 h^{-1}	0.11 h^{-1}

Table 3.2: Concentration of most abundant fermentation products in final sample.

The growth rates in Table 3.2 show some variation, with the highest growth rate observed in fermentation Aa1. This result may be attributed to the addition of 8.3 mM acetic acid in that fermentation,

potentially enhancing mass transfer. However, the reliability of the growth rate calculation, detailed in Appendix H, raises concerns. For Ref1, Ref2, and Ref3, the calculation is based on the initial part of the exponential growth phase, while the calculation for Aa1 relies on the final part. In none of the batch processes, the exponential growth phase was fully captures. Besides, the calibration curves between dry weight and OD_{660} do not met the guideline of acquiring five data points (Appendix H).

Despite the difference in growth rate, no significant differences in fermentation performance were observed, as indicated by comparable biomass concentrations and product yields.

Bubble size and k_La

During the fermentation processes, bubble diameters were measured using the fiber probe. The geometric mean values indicate that the bubble sizes remained relatively constant throughout the experiment (Figure 3.6). However, for the fermentations Ref1 and Ref3, the bubble data was limited (details in Appendix E), causing some deviation. Ref2 was conducted simultaneously with Ref3, and due to the use of a single fiber probe, bubble sizes were not measured. To further support the observation of consistent bubble sizes, violin plots were generated and provided in Appendix E.

The bubble sizes measured during fermentation Aa1 were larger compared to the other fermentations. A different fiber probe position could clarify this result, but for all fermentations the used height and top plate hole were consistent. Besides, since Figure 3.1 demonstrates a decrease in bubble size with increasing acetic acid concentrations, the addition of this compounds is unlikely to be the cause. As fermentation broth are complex systems, further research is needed to explain this inconsistency.

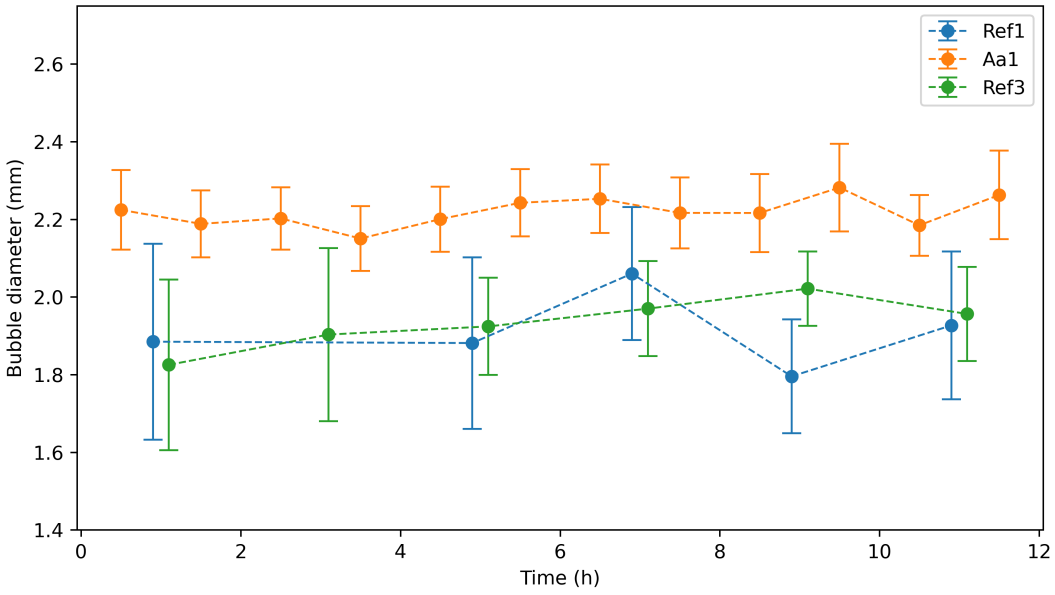

Figure 3.6: Geometric mean bubble diameters throughout the fermentation processes. The error bars indicate the 95% confidence level.

During the fermentation processes, the k_La was determined experimentally with the dynamic gassing-out method and the dynamic pressure method (Figure 3.7). Fermentation Aa1 occurred primarily overnight, limiting the opportunity to perform k_La measurements. During fermentation Ref2, the DO probe used for the dynamic pressure method exhibited significant noise after autoclaving. As a result, the k_La obtained from this method showed substantial variability, and could not be reliably used to assess the progression of k_La during fermentation.

The dynamic gassing-out method indicated a slight increase in $k_L a$ during the fermentations Ref1 and Ref3. According to Figure 3.6, a increase in interfacial area is not the reason for this. This could be attributed to the amount of volume, which decreases throughout the fermentation as samples were taken. This correlates to the abiotic results obtained in Figure 3.4b, due to a decreasing P/V ratio (Equation 19). Another possible explanation is that the presence of cells enhances mass transfer, as cells consume oxygen in the gas-liquid transfer layer (Volger et al., 2024).

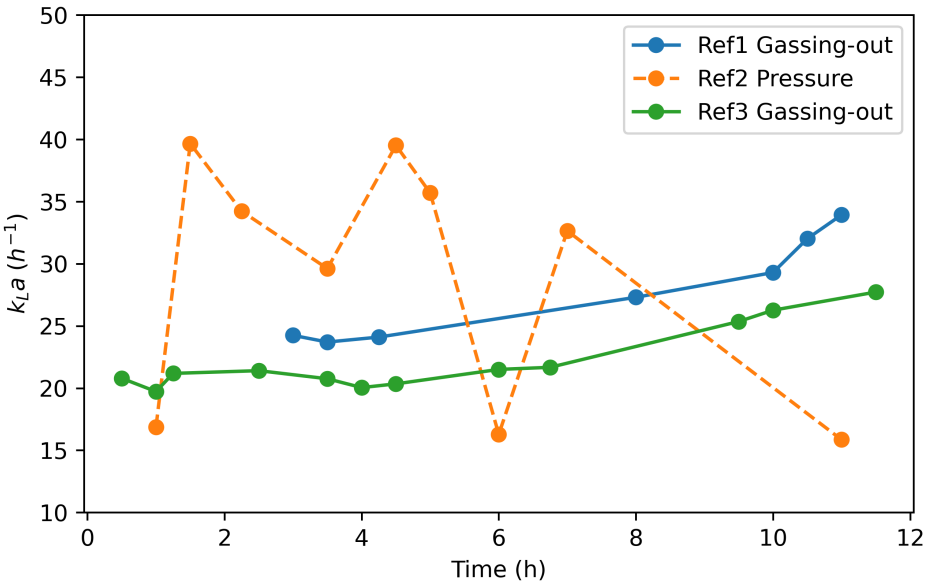

Figure 3.7: Results of $k_L a$ measurements performed during fermentations. The dynamic pressure method and the dynamic gassing-out method was used.

Lastly, the $k_L a$ was also determined using the gaseous oxygen balance method. During fermentation Aa1, a gas leakage occurred in the valve cabinet, and during fermentation Ref2, the noise in the DO data was too severe for this analysis. Therefore, this method could be applied to Ref1 and Ref3, as presented in Figure 3.8. Graphs of the oxygen consumption, $F_{O_2}^{in} - F_{O_2}^{out}$, and the liquid phase oxygen concentration, c_l, used as input for the $k_L a$ calculation (Equation 18), can be found in Appendix I. This calculation is highly sensitive to small deviations in input data, resulting in the spread of data points. Additionally, the initial $k_L a$ values of fermentation Ref1 are unrealistically high, which could be due to the very small driving force in the numerator, as the dissolved oxygen oxygen concentration is still almost at the saturation concentration. To improve the reliability of this methods, additional measurements were performed after Ref1, as explained in Section 1.2.5. This could explain the difference in shape of the graphs between Ref1 and Ref3. During the last part of the exponential growth phase, between 10 and 15 hours, the $k_L a$ values from both fermentations are within the same order of magnitude, around 45 h^{-1}. This value is higher than the results measured with the dynamic gassing-out method, which reports $k_L a$ values between 25 and 35 in that time interval. However, the results from Ref3 exhibit the same rising trend as observed in Figure 3.7.

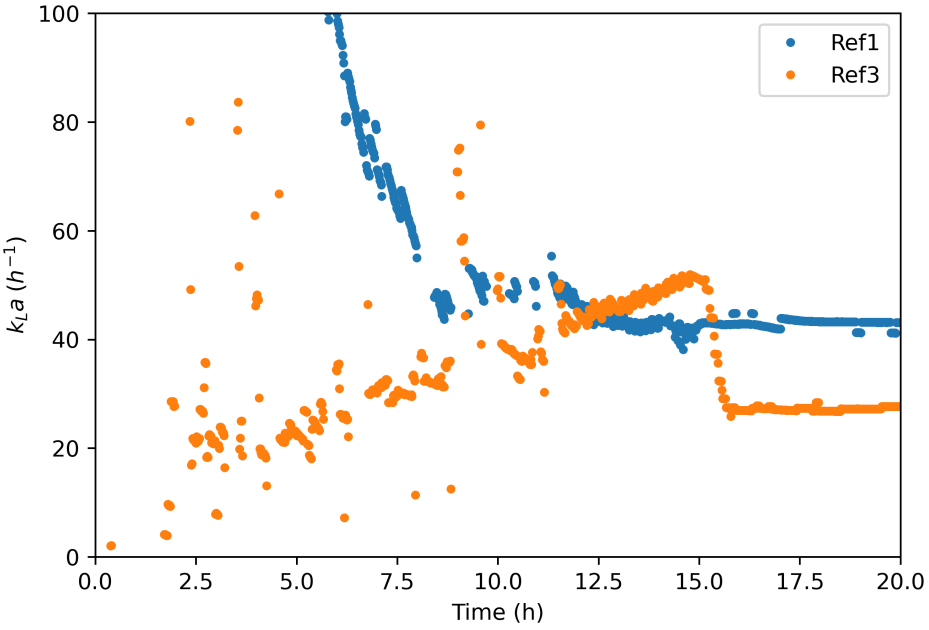

Figure 3.8: Results from k_La determination with the gaseous oxygen balance method.

3.3. Empirical $k_L a$ correlations

In this section is observed whether the experimentally obtained $k_L a$ values exhibit similarity with those predicted by correlations. The used correlations can be found in Section 1.2.7.

3.3.1. Prediction of $k_L a$ for water system

For non-viscous systems, Equation 19 can be applied to calculate the $k_L a$. Previous literature provides various values for the constant C and exponents α and β, as presented in Table 3.5. Using these variables, along with the experimental conditions outlined in Table 2.4, the $k_L a$ was calculated and compared to the experimental values shown in Section 3.1.1 (Figure 3.9).

Author	**C**	α	β	$k_L a$ (h^{-1})
Van't Riet, 1979	$2.6 \cdot 10^{-2}$	0.5	0.4	29.66
Pedersen et al., 1994	$3.9 \cdot 10^{-3}$	0.45	0.67	29.1
Linek et al., 1991	$3.84 \cdot 10^{-3}$	0.4	0.654	36.85
Gagnon et al., 1998	$2.938 \cdot 10^{-3}$	0.504	0.833	38.28
J. M. T. Vasconcelos et al., 2000	$8.3 \cdot 10^{-3}$	0.49	0.62	35.44

Table 3.3: Values for the constant and exponential variables obtained from literature, to predict the $k_L a$ with Equation 19. All authors used Rushton turbines as impellers.

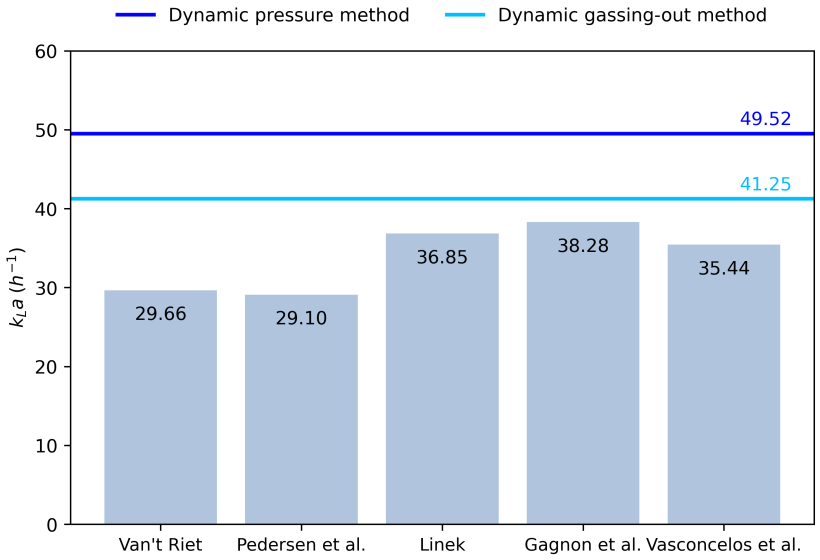

Figure 3.9: Predicted and experimental $k_L a$ values for a water system. The experimental results are discussed in Section 3.1.1.

All predicted $k_L a$ values are lower than the experimental values, indicating that the correlations tend to underpredict the mass transfer rates. Except for Van't Riet (1979), all other studies utilized a working volume at least ten times larger than the volume used in this thesis, which may explain the observed deviations. The correlation proposed by Gagnon et al. (1998) is closest to the experimental values, with a deviation of 7% compared to the dynamic gassing-out method. All predicted values are within a 30% deviation from the value obtained with the dynamic gassing-out method.

3.3.2. Prediction of $k_L a$ during fermentations

To predict $k_L a$ values during a fermentation process, more parameters are used compared to prediction values for water systems. These parameters consist of experimental conditions (Table 2.4), and physical and rheological properties, which are measured from the taken samples from fermentation Ref3 (Table 3.4). The properties from fermentation Ref1 were also measured (Appendix K), but the rheological properties were unreliable and therefore not used for $k_L a$ prediction.

Property		**0 h**	**4 h**	**6 h**	**8 h**	**11 h**
Density	$\rho\ (kg/m^3)$	1018	1012	1033	1015	1014
Volume	$V\ (mL)$	1512	1373	1291	1210	1107
Surface Tension	$\sigma\ (mN/m)$	40.3	40.5	40.9	40.6	40.7
Consistency Index	$k\ (Pa\ s^n)$	0.062	0.049	0.054	0.055	0.061
Flow Behavior Index	n	0.40	0.47	0.51	0.42	0.40
Effective Viscosity: Power-law	$\mu_{eff}\ (mPa\ s)$	4.48	4.74	6.42	4.34	4.54
Effective Viscosity: Casson	$\mu_c\ (mPa\ s)$	1.38	1.63	2.20	1.62	1.51
Effective Viscosity: Perez and Sandall, 1974	$\mu_{eff}\ (mPa\ s)$	5.23	5.46	7.32	5.05	5.29

Table 3.4: Measured physical and rheological properties of fermentation samples from Ref3. The samples were withdrawn from the broth at various time point.

Table 3.4 provides the properties measured from the Ref3 fermentation samples. The density values remain relatively constant, except for the measurement after 6 hours. The volume decrease throughout the fermentation, due to sample collection from the broth. No significant changes in surface tension were observed during the process. Since fermentation broth behaves as a non-Newtonian fluid, the effective viscosity (μ_{eff}) can be described with two rheological models: the Ostwald-de Waele (Power Law) model and the Casson model, discussed in Appendix J. Notably, the calculated μ_{eff} values differ significantly depending on the chosen rheological model. The effective viscosity values indicate that the viscosity of the sample taken after 6 hours is significantly higher than the other samples, which is accompanied by an increased density value. This difference could potentially be attributed to insufficient mixing. However, to ensure that each sample contained well-mixed broth, a pre-sample was collected to flush the sampling tube before taking the actual measurement. For the remaining data, a rising trend in viscosity and density could be expected, due to biomass production, but this was only observed between 0 and 4 hours. Despite some variability in the effective viscosity values, the unprocessed rheology data (Figure J.1) suggest a relatively stable viscosity throughout the fermentation process. This discrepancy could be attributed to the data processing, which is elaborated in Appendix J.

To incorporate the effects of the viscosity in the $k_L a$ prediction, Equation 20 and 21 are proposed by García-Ochoa and Gómez (1998), extending the previously used Equation 19. The constant and exponential variables to be used in the relations depend on the choice of rheological model used (Table 3.5).

Equation	Rheological model	C	α	β	γ
20	Power-law	$6.14 \cdot 10^{-4}$	0.5	0.6	−0.5
20	Casson	$3.97 \cdot 10^{-4}$	0.5	0.6	−0.5
21	Power-law	$2.63 \cdot 10^{-4}$	0.5	2	−0.5
21	Casson	$1.56 \cdot 10^{-4}$	0.5	2	−0.5

Table 3.5: Values for constant and exponential variables obtained from García-Ochoa et al. (2000). They are used to predict the $k_L a$ for fermentation Ref3 with Equation 20 and 21.

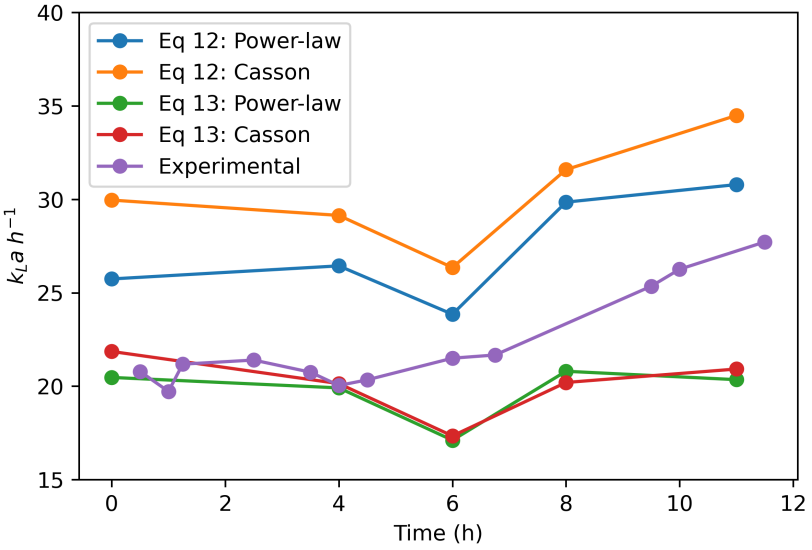

Figure 3.10: Values for $k_L a$ for fermentation Ref3, predicted with Equation 20 and 21. The predicted results can be compared with the experimental data, measured with the dynamic gassing-out method.

The higher viscosity observed in the sample after 6 hours clearly leads to a reduction in $k_L a$ (Figure 3.10). With γ being -0.5, this results follows from Equation 20 and 21. Furthermore, García-Ochoa and Gómez (1998) indicated that increased viscosity reduced surface renewal, thereby decreasing oxygen mass transfer.
Aside from this particular sample, Equation 20 (orange and blue) appears to show a rising trend that correlates with the experimental data. This is likely due to the reduction in volume, which decreases the P/V ratio. Equation 21 does not include a volume parameter and remains relatively constant throughout the process. During the initial part of the fermentation, the predicted values from Equation 21 align closely with the experimental values, determined with the dynamic gassing-out method. All predicted values remain within an error margin of 45% compared to the experimental data. The deviation could be attributed to the variety in impeller. García-Ochoa and Gómez (1998) designed their equations based on a dual six-curve-blade turbine system, while flat blades were used in this study.

The $k_L a$ can also be described with dimensionless correlation, shown in Equations 22, 23, and 24. The parameters to fill in the relations are show in Table 2.4 and 3.4. Each dimensionless correlation used a different rheological model to describe the viscosity.

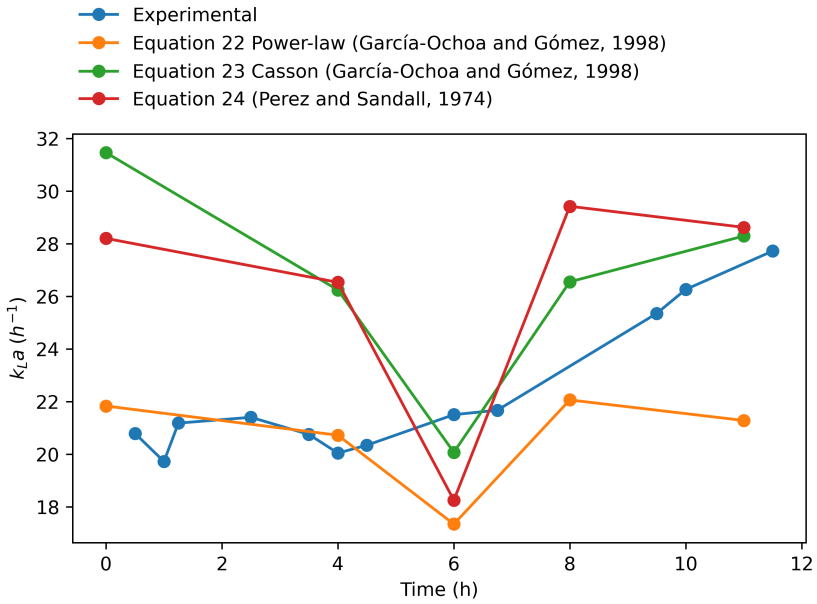

Figure 3.11: Empirical correlations are used to predict $k_L a$ values during fermentation Ref3. The predicted values are compared with the experimental values, measured with the dynamic gassing-out method.

Figure 3.11 highlights the significant impact of viscosity on the prediction models, as evidenced by the pronounced decrease at 6 hours. Beyond this, there is no clear trend among the data points, indicating that the prediction models do not capture the increase in $k_L a$ observed with the dynamic gassing-out method. During the initial phase of fermentation, Equation 22 aligns closely with the experimental values. During the later stages, Equations 23 and 24 provide better alignment. The predicted data remains within a ± 50% error margin compared to the experimental measurements.

4
Conclusion

1. What is the effect of fermentation products (acetic acid, ethanol, and glycerol) on the interfacial area of gas bubbles, and therefore also the oxygen mass transfer ($k_L a$) in a stirred tank reactor?

In aqueous solutions, acetic acid has shown to reduce the bubble size, likely due to the inhibition of bubble coalescence caused by the Marangoni effect (Wang et al., 2024)). This reduction in bubble size leads to an increased interfacial area, thereby enhancing $k_L a$. While ethanol was not examined individually, but literature (Wagenaar, 2021, Puiman, Elisiário, et al., 2022) suggest a similar trend as observed for acetic acid. In contrast, glycerol appeared to have no significant effect on the bubble size and oxygen mass transfer in water.

When bubbles and $k_L a$ are measured in synthetic medium (Table 2.1), notable differences are observed compared to water. This is likely the effect of the antifoam agent Pluronic, which enhances bubble coalescence (McClure et al., 2017). The obtained $k_L a$ value is significantly lower, arguably due to the decreased interfacial area and reduction in k_L. This reduction occurs because the antifoam surfactant molecules hinder oxygen transport across the gas-liquid interface.
The addition of acetic acid, ethanol, and glycerol to synthetic medium solution, which includes glucose and vitamins, does not appear to have a significant effect. It is plausible that other components dominate behavior of bubbles, given the relatively low concentrations of the added organic compounds.

During the conducted fermentation processes, the bubble size remained relatively constant. As fermentation broth is a rather complex system, this could be due to the presence of various components. However, there is no significant increase or decrease in bubble size throughout the fermentation due to the production of acetic acid, ethanol, or glycerol, within the produced concentration rate.
The $k_L a$ measurements show a slight increase throughout the fermentation process. This could be attributed to a decrease in volume, causing a smaller P/V ratio in Equation 19, or to enhanced mass transfer by cells as they consume oxygen in the transfer layer (Volger et al., 2024).

To address the research question: in aqueous solutions, acetic acid and ethanol do reduce bubble size and enhance oxygen mass transfer in a stirred tank reactor. However, within the relatively low concentration range tested, this effect is not observed in synthetic medium or in fermentation broth. The influence of glycerol is negligible.

2. What is the most feasible experimental method to determine the oxygen mass transfer ($k_L a$) in a stirred tank reactor?

In the course of this thesis, three different methods to determine the $k_L a$ have been deployed, as described in Chapter 1.2.5. The initial comparison between the dynamic methods revealed that the pressure-based variant was less stable than the gassing-out method (Table F.1). With the equipment that is currently available within BPE/IMB, stabilizing the pressure at a precise level is challenging, which likely accounts for the minor instability observed. Aside from the initial comparison, other dynamic pressure measurements provided unreliable results due to noise in the DO probe signal, highlighting the need for a sensitive probe. The key advantage of this method - its ability to apply a sudden step-change, which is not guaranteed with the dynamic gassing-out method - is less pronounced in smaller

bioreactors (e.g. 1,5 L).

The dynamic gassing-out method proved to yield stable results and was used to obtain most of the $k_L a$ measurements. Due to its simplicity, applying this method was more efficient than the dynamic pressure method. However, two main limitations must be considered: the response time of the DO probe and the non-ideal mixing of the gas phase. As a result, this method cannot be firmly established as a ground truth without validation against another reliable and well-validated method, such as a chemical technique. It is expected that a correction for the response time is required, before the method will be validated. Nonetheless, it is usable for comparing different experiments and observing the effects of various components in the solution.

As third method, the gaseous oxygen balance method was used to calculate the $k_L a$ in Figure 3.8. This method is very sensitive to errors, and requires very accurate measurement equipment, especially at low oxygen consumption rates. As the $k_L a$ values differ a lot throughout the fermentation processes, the stability of this method is questionable. At the end of the exponential growth phase, Ref3 shows the same rising trend which was obtained with the dynamic gassing-out method, but the values of $k_L a$ are higher (around 45 h^{-1} instead of around 25 h^{-1}). Validation with a reliable method is required to establish a ground truth.

To address the research question: the measurements conducted with the dynamic pressure method and the gaseous oxygen balance method did not yield sufficiently stable results. While they showed potential, further research and methodological improvements are necessary. The dynamic gassing-out method has demonstrated consistency and can be used for comparison between experiments. However, due to its limitations, validation with another reliable $k_L a$ determination method is essential to establish it as ground truth.

3. Is it possible to predict the oxygen mass transfer ($k_L a$) in a stirred tank reactor with empirical correlations within an acceptable deviation range?

Various prediction models were applied to predict $k_L a$ values based on fermentation broth properties and experimental conditions. Predictions for aqueous experiments generally underpredicted the results, but all values were within a 30% deviation from the experimental value (determined with dynamic gassing-out method). In addition to water systems, correlations were used to predict $k_L a$ values during fermentation Ref3. It proved to be challenging to accurately measure rheological properties of the fermentation broth throughout the process. Maintaining a critical perspective on these properties is essential, as they influence the outcomes of the models significantly. The correlations applied to fermentation Ref3 predicted values within an 50% error margin compared to the experimental measurements.

To address the research question: all prediction results in this thesis fall within a 50% error margin from the experimental values. This margin exceeds an acceptable deviation range (Moresi and Patete, 1988) for $k_L a$ predictions used for bioprocess design. Therefore, further research is required to refine the empirical correlations for better alignment with the experimental results, or to explore additional correlations for improved accuracy. Moreover, establishing a reliable ground truth for experimental $k_L a$ determination is essential to enhance any comparison.

5 Recommendations

This section provides recommendations for future research.

Experiments with fermentation products

First, it is recommended to study a broader range of organic compounds produced during fermentation process. Additionally, studying combinations of these compounds would provide insights into potential synergistic effects on bubble coalescence and oxygen mass transfer. This thesis did not examen the impact of individual fermentation broth components (e.g. salts, glucose, antifoam, vitamins). This could bring valuable insights, particularly regarding the observed increase in bubble diameter in synthetic media. In synthetic medium and fermentation broth, the addition and production of acetic acid and ethanol showed no noticeable effects. However, the tested concentration range was relatively low, raising curiosity about the threshold concentration at which these effects might become significant. Incorporating gas holdup results into this research would enable the determination of the interfacial area and the liquid-phase mass transfer coefficient (k_L). These parameters could offer valuable insights into overall oxygen mass transfer by directly correlating it with bubble behavior and mass transfer models.

Experimental $k_L a$ determination

The most important improvement is the need for a ground truth to validate the determination methods used. This would require conducting experiments with reliable and validated chemical methods to provide a benchmark for comparison. For both dynamic methods, a correction for the response time of the probe would enhance the reliability of the measurements. Additionally, the dynamic pressure method and the gaseous oxygen balance method require further development before applying on more experiments.

Empirical $k_L a$ correlations

In this thesis, no predictions have been made for the experiments with organic compounds in water. Adding Newtonian correlations would provide further insights in the effect of these organic compounds on the $k_L a$. For all correlations, but particularly the dimensionless ones, a sensitivity analysis would bring valuable insights into the parameters with the largest impact. It would also provide benchmarks for the required accuracy of fermentation broth property measurements. Collecting more data points by measuring the properties of additional samples could help providing clarity, and support better trending of properties and $k_L a$ prediction. Finally, there are numerous additional (dimensionless) correlations that remain to be explored.

References

A2 Photonic Sensors. (2019, January). *M2 analyzer for bubbles user manual* (v2019-1) [Measurement system and software for particle and bubbly flow analysis]. A2 Photonic Sensors. Grenoble, France. https://www.a2photonicsensors.com

Abubackar, H. N., Veiga, M. C., & Kennes, C. (2011). Biological conversion of carbon monoxide: Rich syngas or waste gases to bioethanol. *Biofuels, Bioproducts and Biorefining*, *5*(1), 93–114. https://doi.org/10.1002/bbb.256

Alves, S., Maia, C., Vasconcelos, J., & Serralheiro, A. (2002). Bubble size in aerated stirred tanks. *Chemical Engineering Journal*, *89*(1-3), 109–117. https://doi.org/10.1016/S1385-8947(02)00008-6

Arjunwadkar, S., Sarvanan, K., Kulkarni, P., & Pandit, A. (1998). Gas-liquid mass transfer in dual impeller bioreactor. *Biochemical Engineering Journal*, *1*(2), 99–106. https://doi.org/10.1016/S1385-8947(97)00083-1

Baird, M., & Davidson, J. (1962). Gas absorption by large rising bubbles. *Chemical Engineering Science*, *17*(2), 87–93. https://doi.org/10.1016/0009-2509(62)80020-7

Bąk, A., & Podgórska, W. (2013). Drop breakage and coalescence in the toluene/water dispersions with dissolved surface active polymers PVA 88% and 98%. *Chemical Engineering Research and Design*, *91*(11), 2142–2155. https://doi.org/10.1016/j.cherd.2013.06.011

Basařová, P., Pišlová, J., Mills, J., & Orvalho, S. (2018). Influence of molecular structure of alcohol-water mixtures on bubble behaviour and bubble surface mobility. *Chemical Engineering Science*, *192*, 74–84. https://doi.org/10.1016/j.ces.2018.07.008

Braasch, H., & Braasch, A. (1934). Unknown. *Ger. Patent*, *605*, 912.

Busti, S., Coccetti, P., Alberghina, L., & Vanoni, M. (2010). Glucose Signaling-Mediated Coordination of Cell Growth and Cell Cycle in Saccharomyces Cerevisiae. *Sensors*, *10*(6), 6195–6240. https://doi.org/10.3390/s100606195

Calderbank, P. H., & Chandrasekharan, K. (1981). Further Observation on the Scale-up of Aerated Mixing Vessels. *Chemical Engineering Science*, *36*, 819–823.

Casey, E., Mosier, N. S., Adamec, J., Stockdale, Z., Ho, N., & Sedlak, M. (2013). Effect of salts on the Co-fermentation of glucose and xylose by a genetically engineered strain of Saccharomyces cerevisiae. *Biotechnology for Biofuels*, *6*(1), 83. https://doi.org/10.1186/1754-6834-6-83
0.5 M.

Cerri, M. O., Esperanca, M. N., Badino, A. C., & Perencin de Arruda Ribeiro, M. (2016). A new approach for kLa determination by gassing-out method in pneumatic bioreactors. *J Chem Technol Biotechnol*, *91*(3061 - 3069).

Chang, H., Halard, B., & Moo-Young, M. (1989). Measurement of kLa by a gassing-in method with oxygen-enriched air. *Biotechnology and Bioengineering*, *34*, 1147–1157.

Chen, P., Sanyal, J., & Duduković, M. (2005). Numerical simulation of bubble columns flows: Effect of different breakup and coalescence closures. *Chemical Engineering Science*, *60*(4), 1085–1101. https://doi.org/10.1016/j.ces.2004.09.070

Chen, S., Timmons, M. B., Aneshansley, D. J., & Bisogni, J. J. (1992). Bubble size distribution in a bubble column applied to aquaculture systems. *Aquacultural Engineering*, *11*(4), 267–280. https://doi.org/10.1016/0144-8609(92)90009-M

Chung, B. T.-f. (1968). Models of some transport processes based on the surface renewal and penetration concept. *Kansas State University*.

Cruz, A., Silva, A., Araujo, M., Giorgano, R., & Hokka, C. (1999). Estimation of the volumetric oxygen tranfer coefficient (KLa) from the gas balance and using a neural network technique. *Braz. J. Chem. Eng.*, *16*. https://www.scielo.br/j/bjce/a/PhZ6jMCtKX6vDXRFzFs7DzD/?lang=en

Dai, Y., Deng, T., Wang, J., & Xu, K. (2004). Enhancement of oxygen gas–liquid mass transfer with colloidal gas aphron dispersions. *Colloids and Surfaces A: Physicochemical and Engineering Aspects*, *240*(1-3), 165–171. https://doi.org/10.1016/j.colsurfa.2004.03.018

Danckwerts, P. V. (1951). Significance of Liquid-Film Coefficients in Gas Absorption. *Industrial and Engineering Chemistry*, *43*(6).

Dang, N. D. P., Karrer, D. A., & Dunn, I. J. (1977). Oxygen transfer coefficients by dynamic model moment analysis. *Biotechnology and Bioengineering*, *19*(6), 853–865. https://doi.org/10.1002/bit.260190606

de Hulster, E. (2011, April). Preparation of Trace element Solution (5 Liter).

de Hulster, E. (2019a, January). Protocol for preparation of synthetic media for Continuous Culture of S. cerevisiae.

de Hulster, E. (2019b, April). Preparation of Vitamin Solution (2 Liter).

Doran, P. M. (2013). In *Bioprocess Engineering Principles* (Second Edition, p. i). Elsevier. https://doi.org/10.1016/B978-0-12-220851-5.00016-2

Duignan, T. T. (2021). The surface potential explains ion specific bubble coalescence inhibition. *Journal of Colloid and Interface Science*, *600*, 338–343. https://doi.org/10.1016/j.jcis.2021.04.144

Elibol, M. (1999). Mass transfer characteristics of yeast fermentation broth in the presence of pluronic F-68. *Process Biochemistry*, *34*(6-7), 557–561. https://doi.org/10.1016/S0032-9592(98)00126-5

Elisiário, M. P., De Wever, H., Van Hecke, W., Noorman, H., & Straathof, A. J. J. (2022). Membrane bioreactors for syngas permeation and fermentation. *Critical Reviews in Biotechnology*, *42*(6), 856–872. https://doi.org/10.1080/07388551.2021.1965952

Franz, K., Buchholz, R., & Schüerl, K. (1980). Comprehensive study of the gas holdup and bubble size distribution in highly viscous liquids I. Glycerol solutions. *Chemical Engineering Communications*, *5*(1-4), 165–186. https://doi.org/10.1080/00986448008935962

Gagnon, H., Lounès, M., & Thibault, J. (1998). Power Consumption and Mass Transfer in Agitated Gas-Liquid Columns: A Comparative Study. *The Canadian Journal of Chemical Engineering*, *76*.

Garcia-Ochoa, F., & Gomez, E. (2005). Prediction of gas-liquid mass transfer coefficient in sparged stirred tank bioreactors. *Biotechnology and Bioengineering*, *92*(6).

Garcia-Ochoa, F., & Gomez, E. (2009). Bioreactor scale-up and oxygen transfer rate in microbial processes: An overview. *Biotechnology Advances*, *27*(2), 153–176. https://doi.org/10.1016/j.biotechadv.2008.10.006

Garcia-Ochoa, F., & Gomez, E. (2010, April). Oxygen Transfer Rate Determination: Chemical, Physical and Biological Methods. In *Encyclopedia of Industrial Biotechnology* (1st ed., pp. 1–21). Wiley. https://doi.org/10.1002/9780470054581.eib467

Garcia-Ochoa, F., Gomez, E., Santos, V. E., & Merchuk, J. C. (2010). Oxygen uptake rate in microbial processes: An overview. *Biochemical Engineering Journal*, *49*(3), 289–307. https://doi.org/10.1016/j.bej.2010.01.011

García-Ochoa, F., Castro, E., & Santos, V. (2000). Oxygen transfer and uptake rates during xanthan gum production. *Enzyme and Microbial Technology*, *27*(9), 680–690. https://doi.org/10.1016/S0141-0229(00)00272-6

García-Ochoa, F., & Gómez, E. (1998). Mass Transfer coefficient in stirred tank reactors for xanthan gum solutions. *Biochemical Engineering Journal*.

Giovannettone, J., Tsai, E., & Gulliver, J. (2009). Gas void ratio and bubble diameter inside a deep airlift reactor. *Chemical Engineering Journal*, *149*(1-3), 301–310. https://doi.org/10.1016/j.cej.2008.11.024

Hasan, B. O. (2017). Breakage of drops and bubbles in a stirred tank: A review of experimental studies. *Chinese Journal of Chemical Engineering*, *25*(6), 698–711. https://doi.org/10.1016/j.cjche.2017.03.008

Haycock, P., & Garner, F. (1959). Circulation in liquid drops. *Proc. R. Soc. Lond. A*, *252*, 457–475. https://doi.org/https://doi.org/10.1098/rspa.1959.0166

Heijnen, J., & Van't Riet, K. (1984). Mass transfer, mixing and heat transfer phenomena in low viscosity bubble column reactors. *The Chemical Engineering Journal*, *28*(2), B21–B42. https://doi.org/10.1016/0300-9467(84)85025-X

Higbie, R. (1935). The Rate of Absorption of a Pure Gas into a Still Liquid during Short Periods of Exposure. *AIChE Journal*, *31*, 365–389. https://api.semanticscholar.org/CorpusID:103837015

Hinze, J. O. (1955). Fundamentals of the hydrodynamic mechanism of splitting in dispersion processes. *AIChE Journal*, *1*(3), 289–295. https://doi.org/10.1002/aic.690010303

Hoseini, S., Najafi, G., Ghobadian, B., & Akbarzadeh, A. (2021). Impeller shape-optimization of stirred-tank reactor: CFD and fluid structure interaction analyses. *Chemical Engineering Journal*, *413*, 127497. https://doi.org/10.1016/j.cej.2020.127497

Humphrey, A. E., & Lee, S. E. (1992). Industrial Fermentation: Principles, Processes, and Products. In J. A. Kent (Ed.), *Riegel's Handbook of Industrial Chemistry* (pp. 916–986). Springer Netherlands. https://doi.org/10.1007/978-94-011-7691-0_24

Jamialahmadi, M., & Müller-Steinhagen, H. (1992). Effect of alcohol, organic acid and potassium chloride concentration on bubble size, bubble rise velocity and gas hold-up in bubble columns. *The Chemical Engineering Journal*, *50*(1), 47–56. https://doi.org/10.1016/0300-9467(92)80005-U acids (formic, acetic, propionic) decrease bubble diameter, alcohols do the same.

Janssen, L., & Warmoeskerken, M. (1987). *Transport Phenomena Data Companion*. Edward Arnold. https://books.google.nl/books?id=sPdUAAAAMAAJ

Kawase, Y., & Moo-Young, M. (1990). The effect of antifoam agents on mass transfer in bioreactors. *Bioprocess Engineering*, *5*(4), 169–173. https://doi.org/10.1007/BF00369581

Keitel, G., & Onken, U. (1982). Inhibition of bubble coalescence by solutes in air/water dispersions. *Chemical Engineering Science*, *37*(11), 1635–1638. https://doi.org/10.1016/0009-2509(82)80033-X

Khan, W. (1990). An extension of Danckwerts theoretical surface renewal model to mass transfer at contaminated turbulent interfaces. *Mathematical and Computer Modelling*, *14*, 750–754. https://doi.org/10.1016/0895-7177(90)90282-R

Lefebvre, A., Mezui, Y., Obligado, M., Gluck, S., & Cartellier, A. (2022). A new, optimized Doppler optical probe for phase detection, bubble velocity and size measurements: Investigation of a bubble column operated in the heterogeneous regime. *Chemical Engineering Science*, *250*, 117359. https://doi.org/10.1016/j.ces.2021.117359

Lehrer, I. H. (1971). Gas Hold-Up and Interfacial Area in Sparged Vessels. *Industrial & Engineering Chemistry Process Design and Development*, *10*(1), 37–40. https://doi.org/10.1021/i260037a006

Lemmon, E. W., & Jacobsen, R. T. (2004). Viscosity and Thermal Conductivity Equations for Nitrogen, Oxygen, Argon, and Air. *International Journal of Thermophysics*, *25*(1), 21–69. https://doi.org/10.1023/B:IJOT.0000022327.04529.f3

Lewis, W. K., & Whitman, W. G. (1924). Principles of Gas Absorption. [_eprint: https://doi.org/10.1021/ie50180a002]. *Industrial & Engineering Chemistry*, *16*(12), 1215–1220. https://doi.org/10.1021/ie50180a002

Li, T., Chen, X.-b., Chen, J.-c., Wu, Q., & Chen, G.-Q. (2014). Open and continuous fermentation: Products, conditions and bioprocess economy. *Biotechnology Journal*, *9*(12), 1503–1511. https://doi.org/10.1002/biot.201400084

Liao, Y., & Lucas, D. (2018). Evaluation of Interfacial Heat Transfer Models for Flashing Flow with Two-Fluid CFD. *Fluids*, *3*(2), 38. https://doi.org/10.3390/fluids3020038

Linek, V., Beneš, P., & Vacek, V. (1989). Dynamic pressure method for kla measurement in large-scale bioreactor. *Biotechnology and Bioengineering*, *33*, 1406–1412.

Linek, V., Sinkule, J., & Beneš, P. (1991). Critical assessment of gassing-in methods for measuring kLa in fermentors. *Biotechnology and Bioengineering*, *38*, 323–330.

Lu, J., Corvalan, C. M., Chew, Y. J., & Huang, J.-Y. (2019). Coalescence of small bubbles with surfactants. *Chemical Engineering Science*, *196*, 493–500. https://doi.org/10.1016/j.ces.2018.11.002

Martín, M., Montes, F. J., & Galán, M. A. (2008a). Bubbling process in stirred tank reactors I: Agitator effect on bubble size, formation and rising. *Chemical Engineering Science*.

Martín, M., Montes, F. J., & Galán, M. A. (2008b). Influence of Impeller Type on the Bubble Breakup Process in Stirred Tanks. *Industrial & Engineering Chemistry Research*, *47*(16), 6251–6263. https://doi.org/10.1021/ie800063v

McClure, D. D., Lamy, M., Black, L., Kavanagh, J. M., & Barton, G. W. (2017). An experimental investigation into the behaviour of antifoaming agents. *Chemical Engineering Science*, *160*, 269–274. https://doi.org/10.1016/j.ces.2016.11.033

McNeil, B., & Harvey, L. M. (1993). Viscous Fermentation Products. *Critical Reviews in Biotechnology*, *13*(4), 275–304. https://doi.org/10.3109/07388559309075699

Mishra, S., & Upadhyay, R. K. (2022). Mass transfer by molecular diffusion. In *Nanotechnology for CO2 Utilization in Oilfield Applications* (pp. 99–125). Elsevier. https://doi.org/10.1016/B978-0-323-90540-4.00003-X

Mohagheghian, S., & Elbing, B. (2018). Characterization of Bubble Size Distributions within a Bubble Column. *Fluids*, *3*(1), 13. https://doi.org/10.3390/fluids3010013

Morão, A., Maia, C. I., Fonseca, M. M. R., Vasconcelos, J. M. T., & Alves, S. S. (1999). Effect of antifoam addition on gas-liquid mass transfer in stirred fermenters. *Bioprocess Engineering*, *20*(2), 165. https://doi.org/10.1007/s004490050576

Moresi, M., & Patete, M. (1988). Prediction of k_L *a* in conventional stirred fermenters. *Journal of Chemical Technology & Biotechnology*, *42*(3), 197–210. https://doi.org/10.1002/jctb.280420304

Morsi, B. I., & Basha, O. M. (2015). Mass Transfer in Multiphase Systems [Section: 9]. In M. Solecki (Ed.), *Mass Transfer*. IntechOpen. https://doi.org/10.5772/60516

Moutafchieva, D., Popova, D., Dimitrova, M., & Tchaoushev, S. (2013). EXPERIMENTAL DETERMINATION OF THE VOLUMETRIC MASS TRANSFER COEFFICIENT.

Muregi, M., Abolarin, M., Okegbile, O., & Eterigho, E. (2021). Influence of temperature and speed on fermentation process during production of bioethanol fuel from cassava. *International Journal of Engineering and Advanced Technology Studies*, *9*(3), 40–46.

Nachtigall, S., Zedel, D., Maass, S., Walle, A., Schäfer, M., & Kraume, M. (2012). Determination of drop breakage mechanisms by experimental and numerical investigations of single drop breakages. *14th European Conference on Mixing, 10–13 September, Warsaw, Poland*.

Nambiar, D. K. R., Kumar, R., & Gandhi, K. S. (1990). Breakage and coalescence of drops in turbulent stirred dispersions. *Sadhana*, *15*(2), 73–103. https://doi.org/10.1007/BF02760469

Newton, J. M., Vlahopoulou, J., & Zhou, Y. (2017). Investigating and modelling the effects of cell lysis on the rheological properties of fermentation broths. *Biochemical Engineering Journal*, *121*, 38–48. https://doi.org/10.1016/j.bej.2017.01.009

NPTEL. (2013). Module 3: Mass Transfer Coefficients.

Otterstedt, K., Larsson, C., Bill, R. M., Ståhlberg, A., Boles, E., Hohmann, S., & Gustafsson, L. (2004). Switching the mode of metabolism in the yeast *Saccharomyces cerevisiae*. *EMBO reports*, *5*(5), 532–537. https://doi.org/10.1038/sj.embor.7400132

Özbek, B., & Gayik, S. (2001). The studies on the oxygen mass transfer coefficient in a bioreactor. *Process Biochemistry*, *36*(8-9), 729–741. https://doi.org/10.1016/S0032-9592(00)00272-7

Pedersen, A. G., Andersen, H., Nielsen, J., & Villadsen, J. (1994). A novel technique based on 85Kr for quantification of gas-liquid mass transfer in bioreactors. *Technical University of Denmark, Department of Biotechnology*, *49*(6), 803–810.

Perez, J. F., & Sandall, O. C. (1974). Gas absorption by non-Newtonian fluids in agitated vessels. *University of California, Department of Chemical and Nuclear Engineering*, *20*(4), 770–775.

Perlmutter, D. (1961). Surface-renewal models in mass transfer. *Chemical Engineering Science*, *16*(3-4), 287–296. https://doi.org/10.1016/0009-2509(61)80039-0

Phillips, J., Huhnke, R., & Atiyeh, H. (2017). Syngas Fermentation: A Microbial Conversion Process of Gaseous Substrates to Various Products. *Fermentation*, *3*(2), 28. https://doi.org/10.3390/fermentation3020028

Prince, M., & Blanch, H. (1990). Bubble coalescence and break-up in air-sparged bubble columns. *AIChE Journal*, *36*, 1485–1499.

Prins, A., & Van'T Riet, K. (1987). Proteins and surface effects in fermentation: Foam, antifoam and mass transfer. *Trends in Biotechnology*, *5*(11), 296–301. https://doi.org/10.1016/0167-7799(87)90080-1

Puiman, L., Abrahamson, B., Lans, R. G. V. D., Haringa, C., Noorman, H. J., & Picioreanu, C. (2022). Alleviating mass transfer limitations in industrial external-loop syngas-to-ethanol fermentation. *Chemical Engineering Science*, *259*, 117770. https://doi.org/10.1016/j.ces.2022.117770

Puiman, L., Elisiário, M. P., Crasborn, L. M., Wagenaar, L. E., Straathof, A. J., & Haringa, C. (2022). Gas mass transfer in syngas fermentation broths is enhanced by ethanol. *Biochemical Engineering Journal*, *185*, 108505. https://doi.org/10.1016/j.bej.2022.108505

Rivas-Interián, R. M., Guillén-Francisco, J. A., Sacramento-Rivero, J. C., Zitlalpopoca-Soriano, Á. G., & Baz-Rodríguez, S. A. (2019). Concentration effects of main components of synthetic culture media on oxygen transfer in bubble column bioreactors. *Biochemical Engineering Journal*, *143*, 131–140. https://doi.org/10.1016/j.bej.2018.12.008

Rommens, S. (2024). Effect of Salts on Gas Bubble Sizes. *Technical University of Delft*.

Rutherford, K., Lee, K., Mahmoudi, S., & Yianneskis, M. (1996). Hydrodynamic characteristics of dual rushton impeller stirred vessels. *AIChE Journal*, *42*(2), 332–346.

Samaras, K., Kostoglou, M., Karapantsios, T. D., & Mavros, P. (2014). Effect of adding glycerol and Tween 80 on gas holdup and bubble size distribution in an aerated stirred tank. *Colloids and Surfaces A: Physicochemical and Engineering Aspects*, *441*, 815–824. https://doi.org/10.1016/j.colsurfa.2013.02.031

Saravanan, K., Ramamurthy, V., & Chandramohan, K. (2009). Gas Hold up in Multiple Impeller Agitated Vessels. *Modern Applied Science*, *3*(2), p49. https://doi.org/10.5539/mas.v3n2p49

Sathyagal, A., Ramkrishna, D., & Narsimhan, G. (1996). Droplet breakage in stirred dispersions. Breakage functions from experimental drop-size distributions. *Chemical Engineering Science*, *51*(9), 1377–1391. https://doi.org/10.1016/0009-2509(95)00311-8

Scargiali, F., Busciglio, A., Grisafi, F., & Brucato, A. (2010). Simplified dynamic pressure method for measurement in aerated bioreactors. *Biochemical Engineering Journal*, *49*(2), 165–172. https://doi.org/10.1016/j.bej.2009.12.008

Sherwood, T. K. (1974). The development of mass transfer theory. *University of California*.

Shewale, S. D., & Pandit, A. B. (2020). Multiphase Phenomena and Design of Gas-Liquid Stirred Tanks. In G. H. Yeoh & J. B. Joshi (Eds.), *Handbook of Multiphase Flow Science and Technology* (pp. 1–53). Springer Nature Singapore. https://doi.org/10.1007/978-981-4585-86-6_47-1

Shimizu, K., Minekawa, K., Hirose, T., & Kawase, Y. (1999). Drop breakage in stirred tanks with Newtonian and non-Newtonian ¯uid systems. *Chemical Engineering Journal*.

Straathof, A. J., & Heijnen, J. (2020, March). Chemical Biotechnology MST-CBT.

Taghavi, M., Zadghaffari, R., Moghaddas, J., & Moghaddas, Y. (2011). Experimental and CFD investigation of power consumption in a dual Rushton turbine stirred tank. *Chemical Engineering Research and Design*, *89*(3), 280–290. https://doi.org/10.1016/j.cherd.2010.07.006

Takahashi, K., & Nienow, A. (1993). Bubble sized and coalescence rates in an aerated vessel agitated by a rushton turbine. *Journal of Chemical Engineering of Japan*.

Tao, F., Ning, S., Zhang, B., Jin, H., & He, G. (2019). Simulation Study on Gas Holdup of Large and Small Bubbles in a High Pressure Gas–Liquid Bubble Column. *Processes*, *7*(9), 594. https://doi.org/10.3390/pr7090594

Treybal, R. E. (1955). *Mass Transfer Operations*. McGraw-Hill.

Tribe, L. A., Briens, C. L., & Margaritis, A. (1995). Determination of the volumetric mass transfer coefficient ($k_L a$) using the dynamic “gas out–gas in” method: Analysis of errors caused by dissolved oxygen probes. *Biotechnology and Bioengineering*, *46*(4), 388–392. https://doi.org/10.1002/bit.260460412

Tsao, G. T. (1968). Simultaneous gas–liquid interfacial oxygen absorption and biochemical oxidation. *Biotechnology and Bioengineering*, *10*(6), 765–785. https://doi.org/https://doi.org/10.1002/bit.260100605

Urban, A. L., Hettiarachchi, S. L., Miller, K. F., Kincaid, G. P., & Gulliver, J. S. (2001). Field Experiments to Determine Gas Transfer at Gated Sills. *Journal of Hydraulic Engineering*, *127*(10), 848–859. https://doi.org/10.1061/(ASCE)0733-9429(2001)127:10(848)

van der Bom, J. (2023). Bubble property determination: Comparison between bubble data from a fiber probe, and a camera. *Bioprocess Engineering, Technical University of Delft*.

Van’t Riet, K. (1979). Review of Measuring Methods and Results in Nonviscous Gas-Liquid Mass Transfer in Stirred Vessels. *Industrial & Engineering Chemistry Process Design and Development*, *18*(3), 357–364. https://doi.org/10.1021/i260071a001

Vasconcelos, J., Rodrigues, J., Orvalho, S., Alves, S., Mendes, R., & Reis, A. (2003). Effect of contaminants on mass transfer coefficients in bubble column and airlift contactors. *Chemical Engineering Science*, *58*(8), 1431–1440. https://doi.org/10.1016/S0009-2509(02)00675-9

Vasconcelos, J. M. T., Orvalho, S. C. P., Rodrigues, A. M. A. F., & Alves, S. S. (2000). Effect of Blade Shape on the Performance of Six-Bladed Disk Turbine Impellers. *Industrial & Engineering Chemistry Research*, *39*(1), 203–213. https://doi.org/10.1021/ie9904145

Verma, P. (Ed.). (2022). *Industrial Microbiology and Biotechnology*. Springer Singapore. https://doi.org/10.1007/978-981-16-5214-1

Volger, R., Puiman, L., & Haringa, C. (2024). Bubbles and Broth: A review on the impact of broth composition on bubble column bioreactor hydrodynamics. *Biochemical Engineering Journal*, *201*, 109124. https://doi.org/10.1016/j.bej.2023.109124

Vos, T., De La Torre Cortés, P., Van Gulik, W. M., Pronk, J. T., & Daran-Lapujade, P. (2015). Growth-rate dependency of de novo resveratrol production in chemostat cultures of an engineered Saccharomyces cerevisiae strain. *Microbial Cell Factories*, *14*(1), 133. https://doi.org/10.1186/s12934-015-0321-6

Wagenaar, E. C. H. (2021). Influence of ethanol on the bubble size and the gas-liquid mass transfer of oxygen. *Bioprocess Engineering, Technical University of Delft*.

Wang, Y., Shen, X., Zhang, H., & Wang, T. (2024). Marangoni effect on hydrodynamics and mass transfer behavior in an internal loop airlift reactor under elevated pressure. *AIChE Journal*, *70*(2), e18291. https://doi.org/10.1002/aic.18291

Warmoeskerken and Smith, M. (1985). Flooding of Disc Turbines in Gas-Liquid Dispersions: A New Description of the Phenomenon. *Chemical Engineering Science*, *40*(11), 2063–2071.

Wei, C.-J., Tanner, R. D., & Malaney, G. W. (1982). Effect of Sodium Chloride on Bakers’ Yeast Growing in Gelatin. *Applied and Environmental Microbiology*, *43*(4), 757–763. https://doi.org/10.1128/aem.43.4.757-763.1982
0.5 M NaCl.

Wen, T., Lu, L., & Luo, Y. (2021). Review on the fundamentals and investigations of falling film dehumidification/absorption refrigeration based on CFD technology. *International Journal of Heat and Mass Transfer*, *171*, 121042. https://doi.org/10.1016/j.ijheatmasstransfer.2021.121042

Xing, W., Yin, M., Lv, Q., Hu, Y., Liu, C., & Zhang, J. (2014). 1 - Oxygen Solubility, Diffusion Coefficient, and Solution Viscosity. In W. Xing, G. Yin, & J. Zhang (Eds.), *Rotating Electrode Methods and Oxygen Reduction Electrocatalysts* (pp. 1–31). Elsevier. https://doi.org/https://doi.org/10.1016/B978-0-444-63278-4.00001-X

Zieminski, S. A., Caron, M. M., & Blackmore, R. B. (1967). Behavior of Air Bubbles in Dilute Aqueous Solutions. *Industrial & Engineering Chemistry Fundamentals*, *6*(2), 233–242. https://doi.org/10.1021/i160022a011

Zieminski, S. A., & Hill, R. L. (1962). Bubble Aeration of Water in the Presence of Some Organic Compounds. *Journal of Chemical & Engineering Data*, *7*(1), 51–54. https://doi.org/10.1021/je60012a014

A

Trace elements & vitamins

Chemicals	Formula	Product Code	Concentration (g/L)
EDTA (Titriplex III®)	$C_{10}H_{14}N_2Na_2O_8 \cdot 2H_2O$	Merck 8418	15.00
Zinc sulfate.7H_2O	$ZnSO_4 \cdot 7H_2O$	Merck 8883	4.50
Manganese (II) chloride.2H_2O	$MnCl_2 \cdot 2H_2O$	Merck 5934	0.84
Cobalt (II) chloride.6H_2O (Toxic)	$CoCl_2 \cdot 6H_2O$	Merck 2539	0.30
Copper (II) sulfate.5H_2O	$CuSO_4 \cdot 5H_2O$	J.T.Baker 0104	0.30
Di-Sodium molybdate.2H_2O	$Na_2MoO_4 \cdot 2H_2O$	Merck 6521	0.40
Calcium chloride.2H_2O	$CaCl_2 \cdot 2H_2O$	Merck 2382	4.50
Iron sulfate.7H_2O	$FeSO_4 \cdot 7H_2O$	J.T.Baker 0126	3.00
Boric acid	H_3BO_3	Merck 0165	1.00
Potassium iodide	KI	Merck 5043	0.10

Table A.1: Chemical composition of trace elements solution used in the experiments (de Hulster, 2011).

Compound	Formula	Product Code	Concentration (g/L)
Biotin (D-)	$C_{10}H_{16}N_2O_3S$	Calbiochem/ Merck 2031	0.05
Ca D(+) pantothenate	$C_{18}H_{32}CaN_2O_{10}$	Sigma 21210	1.00
Nicotinic acid	$C_6H_5NO_2$	Sigma 72309	1.00
Myo-inositol (for microbiology)	$C_6H_{12}O_6$	Merck 4728	25.00
Thiamine chloride hydrochloride	$C_{12}H_{17}ClN_4OS \cdot HCl$	Merck 8181	1.00
Pyridoxine hydrochloride	$C_8H_{11}NO_3 \cdot HCl$	Sigma P6280	1.00
p-aminobenzoic acid	$C_7H_7NO_2$	Merck 0250	0.20

Table A.2: Composition of vitamins solution used in the experiments (de Hulster, 2019b).

B
Fiber probe verification

To validate the use of the fiber probe in a stirred tank reactor, bubble data was collected using both the probe and with a camera. One of the images used for verification is shown on the cover of this thesis. Bubble diameters were determined from the pictures with ImageJ. The data is compared with the bubble size distributions (Figure B.1).

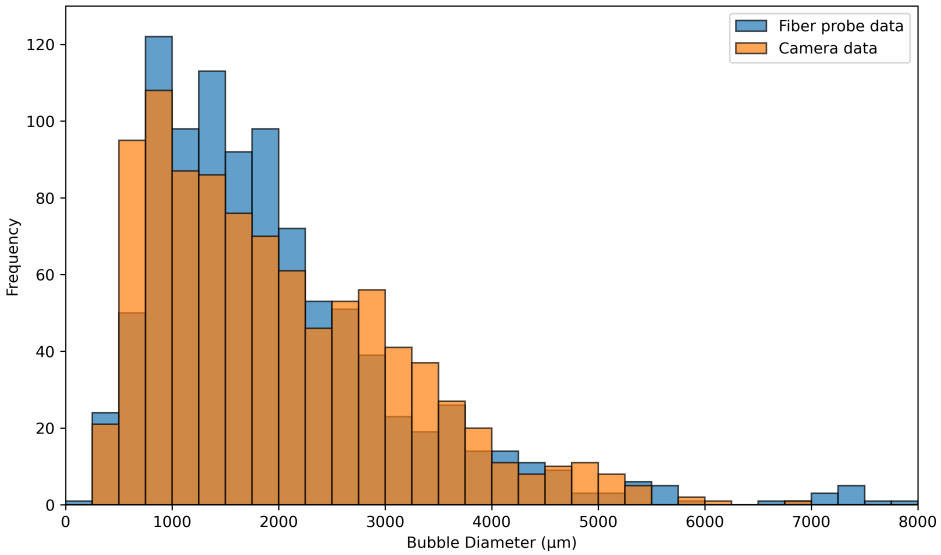

Figure B.1: Bubble size distribution of bubbles measured with the fiber probe and with a camera.

Data Source	Valid bubbles	Geometric means (mm)	Median (mm)	Minimum (mm)	Q1 (mm)	Q3 (mm)	Maximum (mm)
Camera	943	1.67	1.74	0.29	1.04	2.76	10.42
Fiber probe	960	1.66	1.70	0.23	1.10	2.48	9.15

Table B.1: Bubble size details of bubbles measured with the fiber probe and with a camera.

The bubble size distributions (Figure B.1) align reasonably well, and the bubble size details are comparable. These results indicate that the fiber probe is suitable for measuring bubble sizes in a stirred tank reactor.

C

Response time of DO probe

Van't Riet (1979) defined the response time of a dissolved oxygen probe as the time required to records 63% of the full response of a stepwise change in oxygen concentration. This was determined by transferring the probe from a solution with sodium sulfite (Na_2SO_3), whose oxygen concentration is zero, to another solution saturated with air. The probe signal was recorded, showing that it took 17.5 seconds and 16.3 seconds to reach 63% of the final value, as presented in Figures C.1 and C.2.

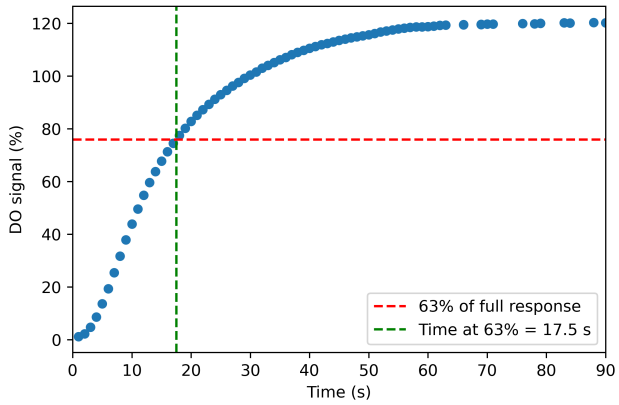

Figure C.1: Response time determination 1

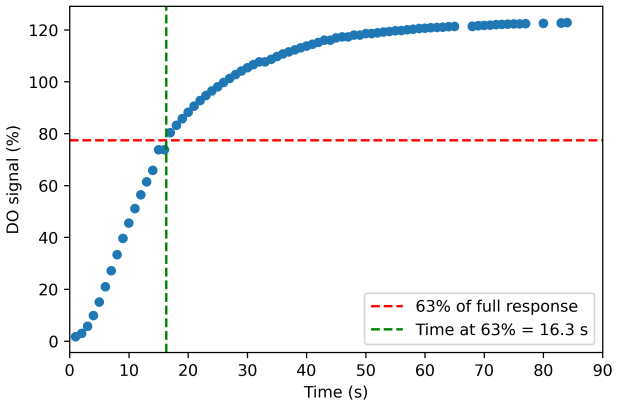

Figure C.2: Response time determination 2

D

Bubble size data processing

Gas bubbles are measured with the fiber probe, as described in Section 1.2.6. When (preferably) over a 1000 valid bubbles are measured with the fiber probe, a bubble size distribution is established. An example of a bubble size distribution is shown in Figure D.1.

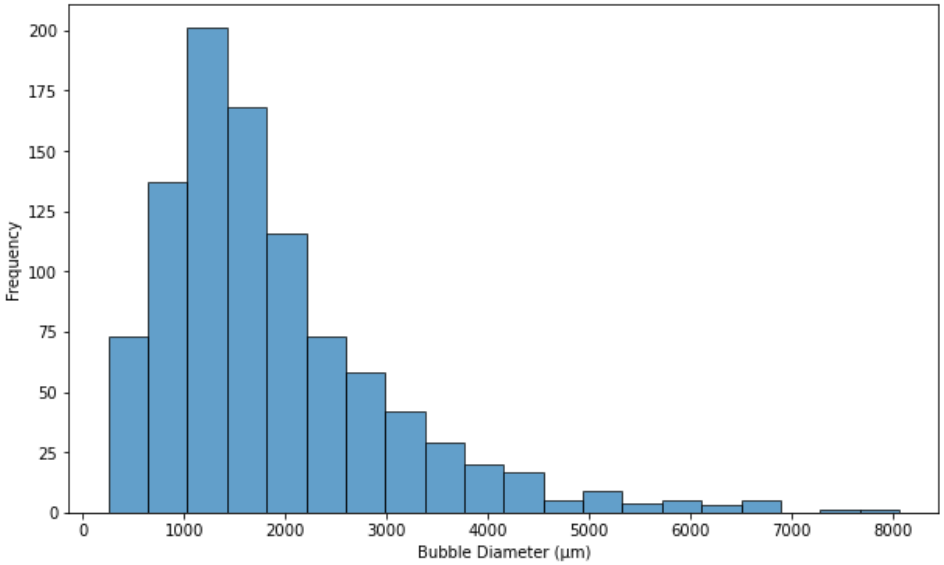

Figure D.1: Bubble size distribution (0.5 mM acetic acid)

To compare different sets of bubble size measurements with each other, violin plots are obtained, as shown in Appendix E. As they are similar to box-plots, the stripes declare the following values: minimum value, first quartile, median, third quartile, and maximum. The width of the plot represents the frequency.

As bubble size distributions are often poly-dispersed, it can be challenging to describe the distribution with a single length scale (Mohagheghian and Elbing, 2018). For the purpose of mass transfer, the bubble size is often described with the Sauter mean diameter, shown in Equation 25 (Puiman, Elisiário, et al., 2022, Martín et al., 2008a).

$$d_{32} = 6 \cdot \frac{\sum V_{b,i}}{\sum A_{b,i}} = 6 \cdot \frac{\frac{4}{3}\pi \sum \left(\frac{1}{2} d_{b,i}\right)^3}{4\pi \sum \left(\frac{1}{2} d_{b,i}\right)^2} = \frac{\sum d_{b,i}^3}{\sum d_{b,i}^2} \tag{25}$$

However, because the particle diameters are cubed in the numerator, larger particles contribute disproportionally more to the total sum compared to smaller particles. Therefore, the Sauter mean diameter is more sensitive to the largest bubbles within the flow (Mohagheghian and Elbing, 2018). As a result, using the Sauter mean diameter did not accurately represent the dataset compared to the violin plots,

primarily due to the presence of a few outliers. As example the bubbles sizes during the fermentation on September 19th are obtained. From the violin plots (D.3) is understood that the bubble diameter is relatively constant throughout the fermentation. However, the Sauter diameter values show quite a deviation throughout the fermentation process (Figure D.3).

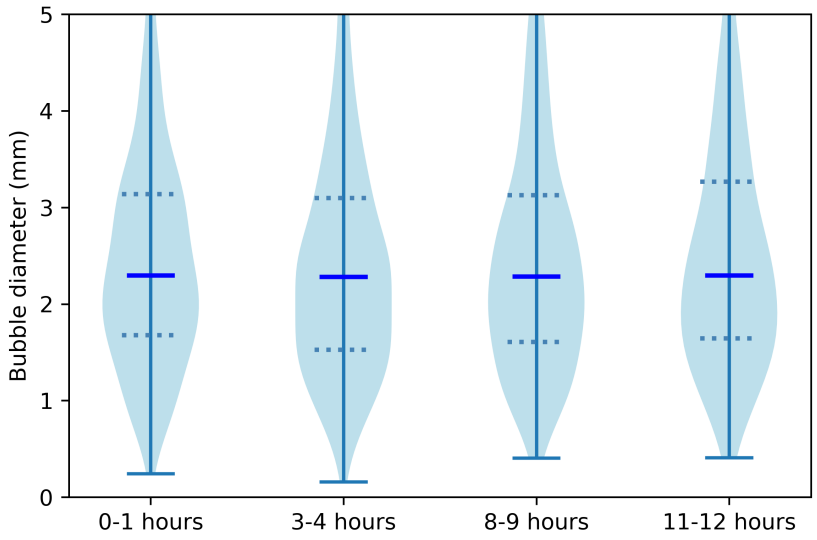

Figure D.2: Bubble data of time slots from the fermentation on September 19th. Only a few time slots are shown to improve the readability.

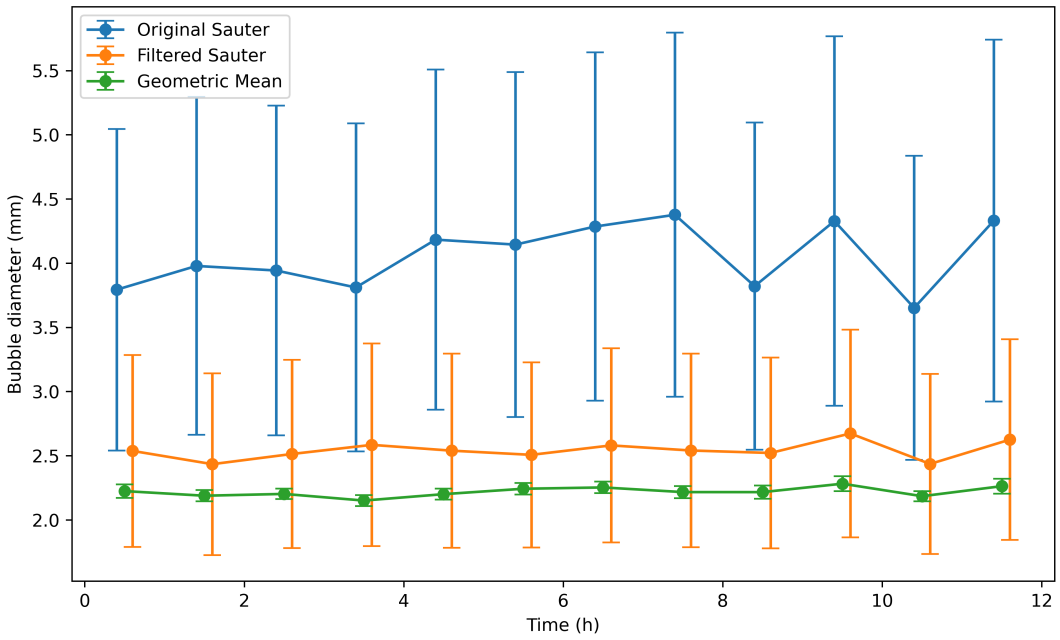

Figure D.3: Bubble size data sets throughout the fermentation on September 19th. The error bars represent the standard deviations for the data sets at different time points.

To improve the representation of the data, large bubbles were removed with an outlier technique proposed by Giovannettone et al. (2009). For every bubble diameter, a z-score was calculated with Equation 26. Every measurement with a z-score above the threshold of $z_s = 2.5$ was not included in the Sauter mean diameter calculation (Urban et al., 2001). The trend of the Sauter diameter of the filtered

data set provided a more accurate presentation, but the standard deviation was still significantly large.

$$z_s = \frac{d_i - median(d_i)}{S} \tag{26}$$

Eventually, the geometric mean (Equation 27) was used as parameter represent the bubble data, reducing the impact of extremely large values and presenting data with a minor standard deviation.

$$Geometric\ mean = \sqrt[n]{d_{b,1} \cdot d_{b,2} \cdots d_{b,n}} \tag{27}$$

E

Bubble size data

E.1. Abiotic experiments

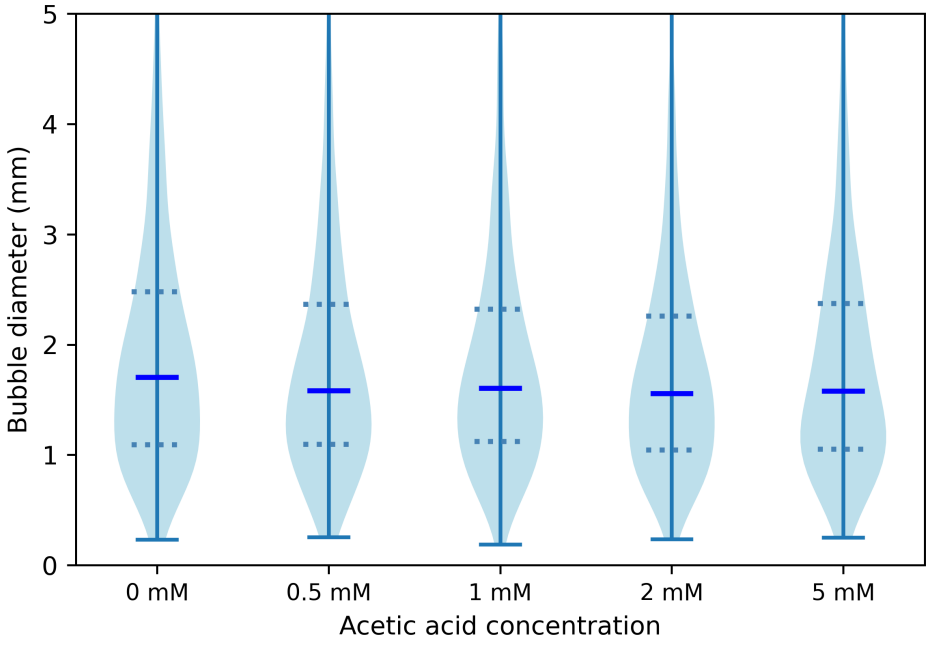

Figure E.1: Bubble data at different acetic acid concentrations. The stripes declare the following values: minimum value, first quartile, median, third quartile, and maximum. The top of the plots is not shown to improve readability, instead the maximum values are provided in Table E.1. The width of the plot represents the frequency.

Acetic acid	Valid bubbles	Geometric means (mm)	Median (mm)	Minimum (mm)	Q1 (mm)	Q3 (mm)	Maximum (mm)
0 mM	961	1.66	1.70	0.23	1.10	2.48	9.15
0.5 mM	967	1.58	1.58	0.25	1.10	2.37	8.06
1 mM	917	1.60	1.61	0.19	1.12	2.32	8.93
2 mM	903	1.55	1.56	0.24	1.05	2.26	8.60
5 mM	774	1.58	1.58	0.25	1.05	2.37	9.77

Table E.1: Bubble size details for different acetic acid concentrations.

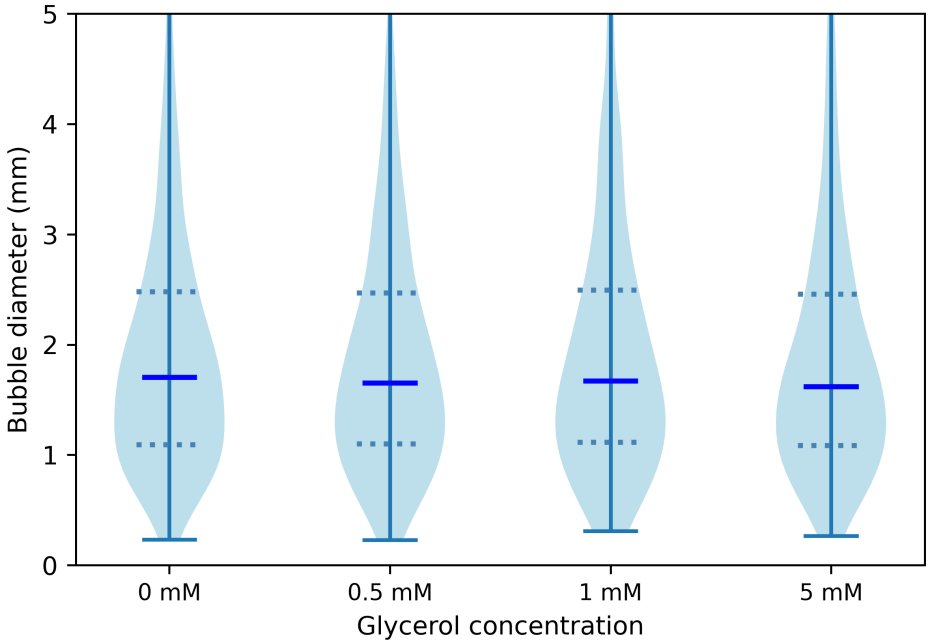

Figure E.2: Bubble data at different glycerol concentrations. The stripes declare the following values: minimum value, first quartile, median, third quartile, and maximum. The top of the plots is not shown to improve readability, instead the maximum values are provided in Table E.2. The width of the plot represents the frequency.

Glycerol (mM)	Valid bubbles	Geometric means (mm)	Median (mm)	Minimum (mm)	Q1 (mm)	Q3 (mm)	Maximum (mm)
0	961	1.66	1.70	0.23	1.10	2.48	9.15
0.5	540	1.65	1.65	0.23	1.10	2.47	8.18
1	724	1.65	1.67	0.31	1.12	2.50	9.74
5	1018	1.62	1.62	0.26	1.09	2.46	9.56

Table E.2: Bubble size details for different glycerol concentrations.

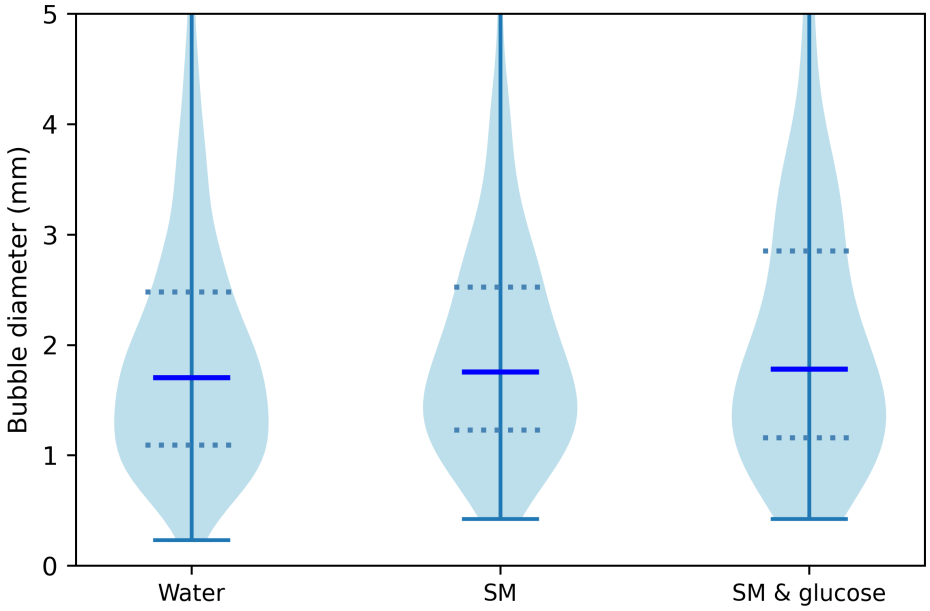

Figure E.3: Bubble data for different solutions: water; synthetic medium; synthetic medium, glucose and vitamins. The exact composition is provided in Table 2.2. The stripes declare the following values: minimum value, first quartile, median, third quartile, and maximum. The top of the plots is not shown to improve readability, instead the maximum values are provided in Table E.3. The width of the plot represents the frequency.

Solution	Valid bubbles	Geometric means (mm)	Median (mm)	Minimum (mm)	Q1 (mm)	Q3 (mm)	Maximum (mm)
Water	961	1.66	1.70	0.23	1.10	2.48	9.15
SM	250	1.73	1.76	0.42	1.23	2.53	7.00
SM & glu	141	1.76	1.78	0.43	1.16	2.85	7.98

Table E.3: Bubble size details for different solutions: water; synthetic medium; synthetic medium, glucose and vitamins. The exact composition is provided in Table 2.2.

E.2. Fermentations

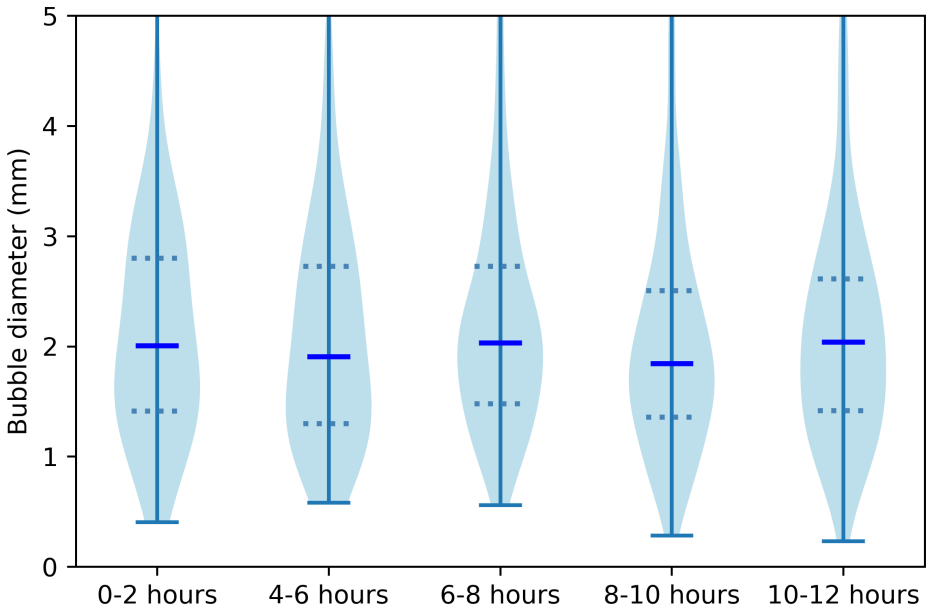

Figure E.4: Bubble data across time interval during fermentation Ref1 shown in violin plots. The stripes declare the following values: minimum value, first quartile, median, third quartile, and maximum. The top of the plots is not shown to improve readability, instead the maximum values are provided in Table E.4. The width of the plot represents the frequency.

Time slots (h)	Valid bubbles	Geometric means (mm)	Median (mm)	Minimum (mm)	Q1 (mm)	Q3 (mm)	Maximum (mm)
0 - 2	76	1.88	2.01	0.40	1.41	2.80	7.82
4 - 6	103	1.88	1.91	0.58	1.30	2.73	6.68
6 - 8	179	2.06	2.03	0.56	1.48	2.73	7.32
8 - 10	199	1.80	1.84	0.28	1.36	2.51	6.01
10 - 12	153	1.93	2.04	0.23	1.42	2.61	7.59

Table E.4: Bubble size details for time intervals during fermentation Ref1.

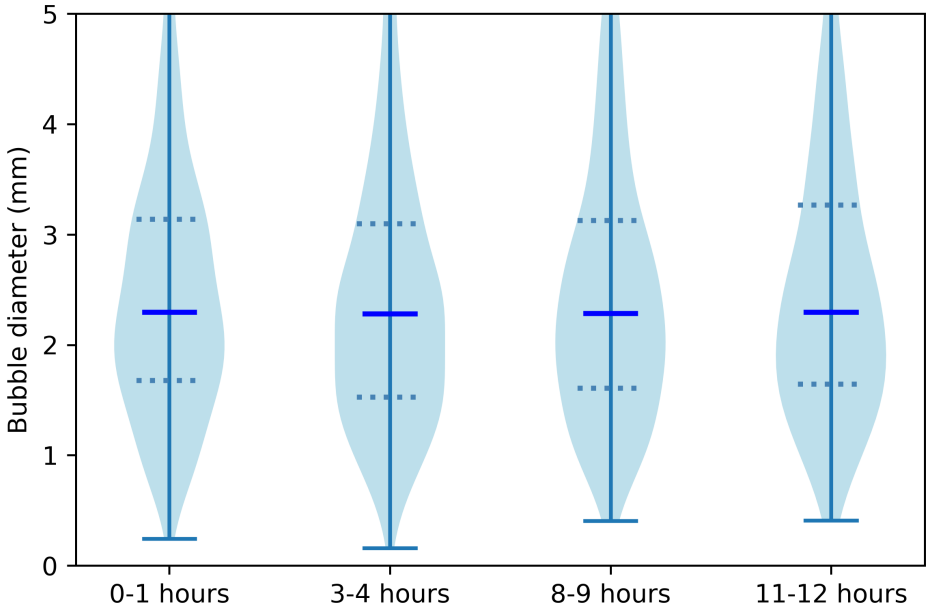

Figure E.5: Bubble data across time interval during fermentation Aa1 shown in violin plots. The stripes declare the following values: minimum value, first quartile, median, third quartile, and maximum. The top of the plots is not shown to improve readability, instead the maximum values are provided in Table E.5. The width of the plot represents the frequency. Only a few time slots are shown to improve the readability.

Time slots (h)	Valid bubbles	Geometric means (mm)	Median (mm)	Minimum (mm)	Q1 (mm)	Q3 (mm)	Maximum (mm)
0 - 1	576	2.22	2.30	0.25	1.68	3.14	7.61
1 - 2	889	2.19	2.24	0.18	1.56	3.07	9.40
2 - 3	988	2.20	2.23	0.35	1.58	3.11	11.66
3 - 4	896	2.15	2.28	0.16	1.53	3.10	7.84
4 - 5	959	2.20	2.26	0.30	1.58	3.16	15.63
5 - 6	929	2.24	2.25	0.50	1.62	3.19	10.52
6 - 7	914	2.25	2.35	0.24	1.65	3.20	14.03
7 - 8	927	2.22	2.29	0.20	1.56	3.10	12.37
8 - 9	618	2.22	2.28	0.41	1.61	3.13	7.38
9 - 10	626	2.28	2.32	0.32	1.59	3.31	11.90
10 - 11	879	2.18	2.25	0.16	1.63	3.14	9.24
11 - 12	588	2.26	2.30	0.41	1.65	3.27	11.85

Table E.5: Bubble size details for time intervals during fermentation Aa1.

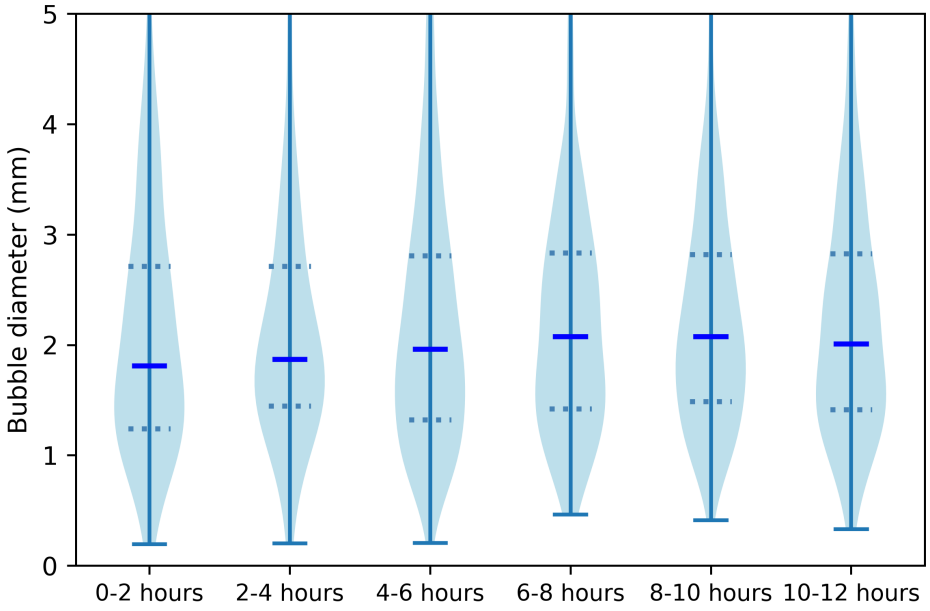

Figure E.6: Bubble data across time interval during fermentation Ref3 shown in violin plots. The stripes declare the following values: minimum value, first quartile, median, third quartile, and maximum. The top of the plots is not shown to improve readability, instead the maximum values are provided in Table E.5. The width of the plot represents the frequency.

Time slots (h)	Valid bubbles	Geometric means (mm)	Median (mm)	Minimum (mm)	Q1 (mm)	Q3 (mm)	Maximum (mm)
0 - 2	97	1.83	1.81	0.20	1.24	2.71	5.71
2 - 4	111	1.90	1.87	0.20	1.45	2.71	8.52
4 - 6	330	1.92	1.96	0.21	1.32	2.81	7.54
6 - 8	285	1.97	2.08	0.47	1.42	2.83	6.78
8 - 10	461	2.02	2.07	0.41	1.49	2.82	8.66
10 - 12	292	1.96	2.01	0.33	1.41	2.83	6.72

Table E.6: Bubble size details for time intervals during fermentation Ref3.

F

Pressure method: acetic acid

The dynamic pressure measurements in Figure 3.2 have relatively large error bars, which are derived from the values in Table F.1.

Acetic acid concentration	**0 mM**	**0.5 mM**	**1 mM**	**2 mM**
	57.8 h^{-1}	77.71 h^{-1} 84.94 h^{-1} 78.59 h^{-1} 67.25 h^{-1} 53.96 h^{-1}	66.46 h^{-1} 58.2 h^{-1}	43.92 h^{-1}
Average	**57.8 h^{-1}**	**72.49 h^{-1}**	**62.33 h^{-1}**	**43.92 h^{-1}**
Standard deviation	-	12.2	5.9	-

Table F.1: Experimental k_La values measured with the dynamic pressure method in different acetic acid concentrations.

The k_La values measured with the dynamic pressure method in 0.5 mM acetic acid solution exhibit some instability. These values are derived by curve fitting from the desorption profiles, created by pressure releases. One of these profiles (Figure F.1b) contains significantly fewer data points compared to the profile in Figure F.1a, which is used for Section 3.1.1. This difference is likely due to the usage of a less sensitive DO probe. As a result, it becomes more challenging to accurately determine the k_La values, leading to a greater variability among measurements under the same conditions.

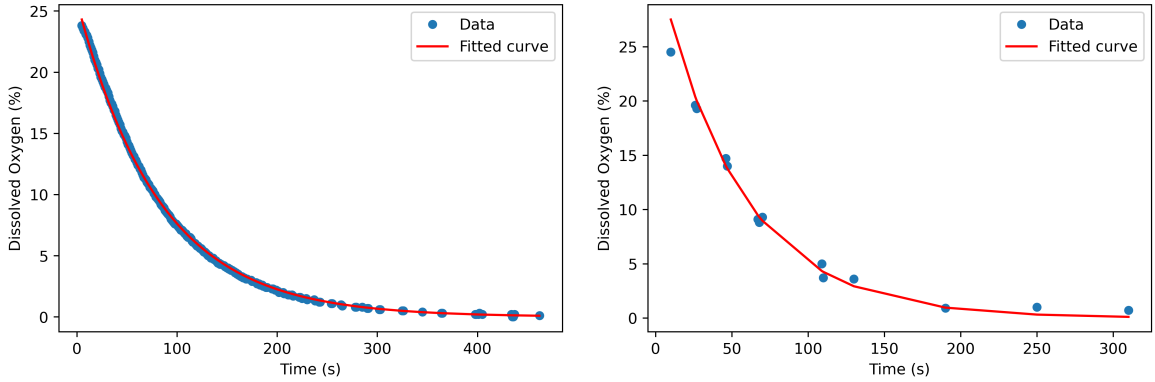

(a) Desorption profile measured with sensitive DO probe. The k_La fitted from the curve is 43.90 h^{-1}.

(b) Desorption profile measured with less sensitive DO probe. The k_La fitted from the curve is 67.25 h^{-1}.

Figure F.1: Desorption profile resulting from a pressure release from 1.2 bar to 1 bar. In practice, the DO values were approximately 100%; however, the curve was shifted toward the x-axis to facilitate curve fitting.

G

Fermentation performance Aa1, Ref2, and Ref3

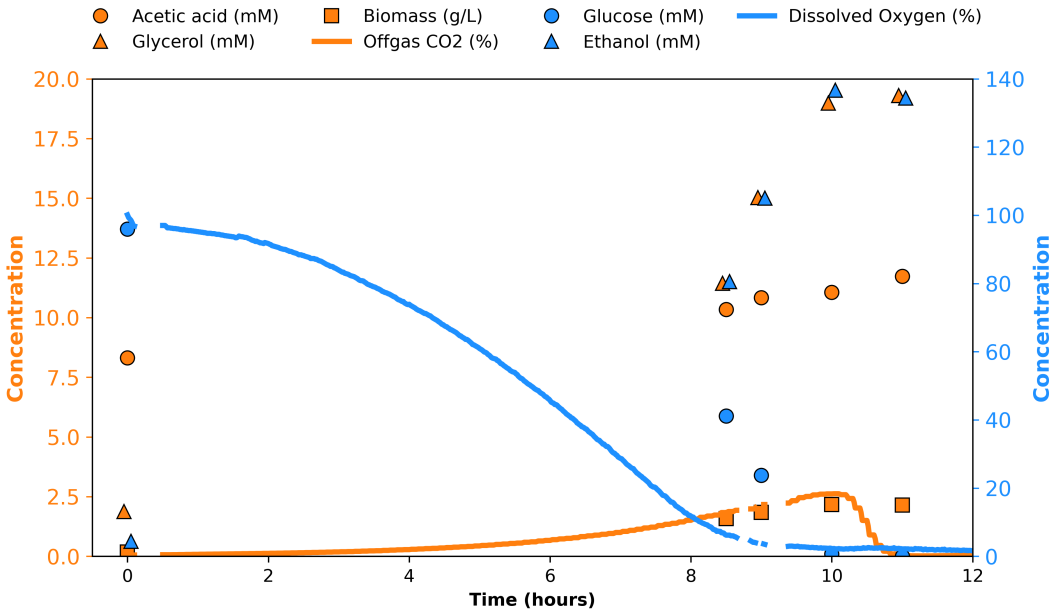

Figure G.1: Concentrations of fermentation broth components and gas fractions throughout batch fermentation Aa1. The orange data corresponds to the left y-axis, and the blue data corresponds to the right y-axis. Fluctuations in the DO and off-gas CO_2 curves caused by dynamic gassing-out measurements were removed for improved readability.

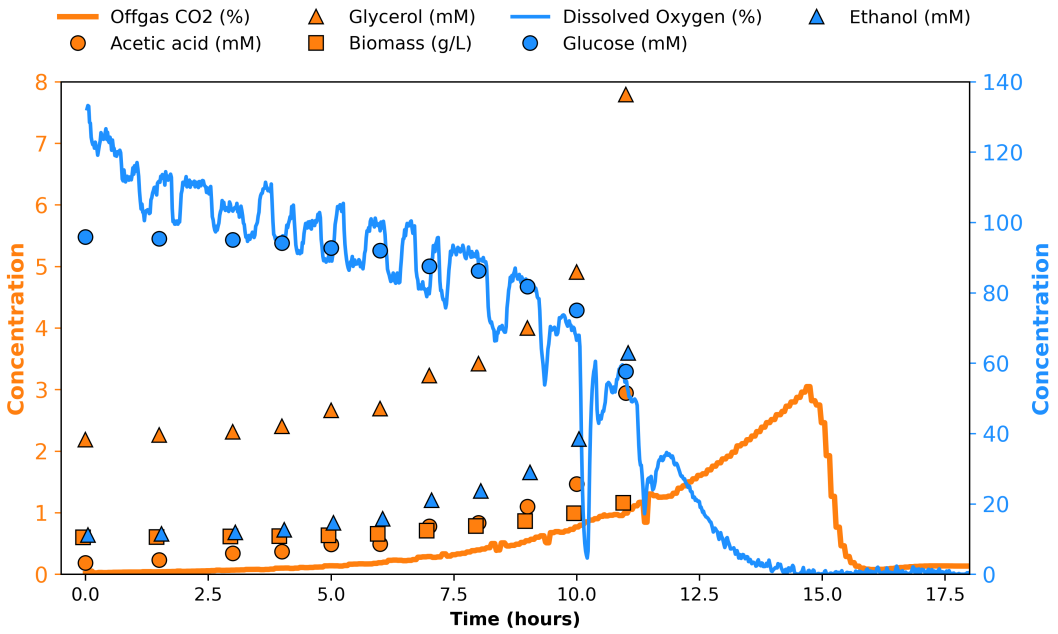

Figure G.2: Concentrations of fermentation broth components and gas fractions throughout batch fermentation Ref2. The orange data corresponds to the left y-axis, and the blue data corresponds to the right y-axis.

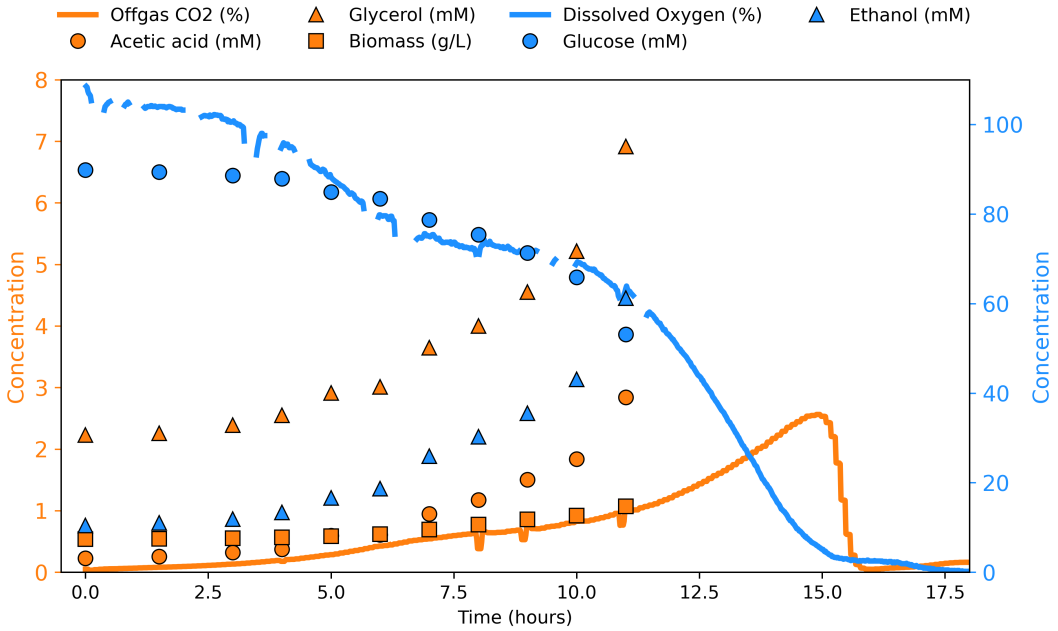

Figure G.3: Concentrations of fermentation broth components and gas fractions throughout batch fermentation Ref1. The orange data corresponds to the left y-axis, and the blue data corresponds to the right y-axis. Fluctuations in the DO curve caused by dynamic gassing-out measurements were removed for improved readability.

H

Growth rate determination

Throughout the fermentation process, biomass concentration was monitored using both OD_{660} and dry weight measurements. While OD can be monitored continuously throughout the fermentation process, dry weight measurements are typically performed only when the OD exceeds a level of 2. When multiple samples are available with both OD and dry weight measurements, a calibration curve can be established (Figure H.1). Although the R^2 values are very close to 1, it is preferable to use at least five data points to create a reliable formula. However, for all batches this guideline was not met.

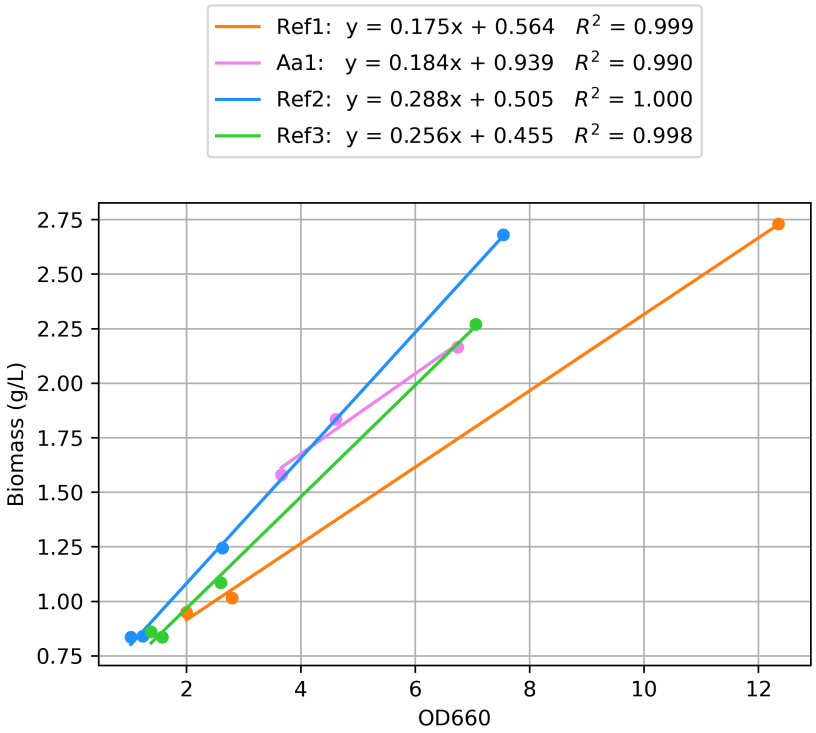

Figure H.1: Calibration curves between dry weight and the OD_{660} measurements, for all fermentation processes. The linear equations and their R^2 are presented.

Subsequently, these calibration curves were applied to calculate the biomass concentrations from the measured OD_{660} values. By taking the natural logarithm, the exponential growth phase (linear segment) could be identified. The slopes of the resulting equations represent the growth rates.

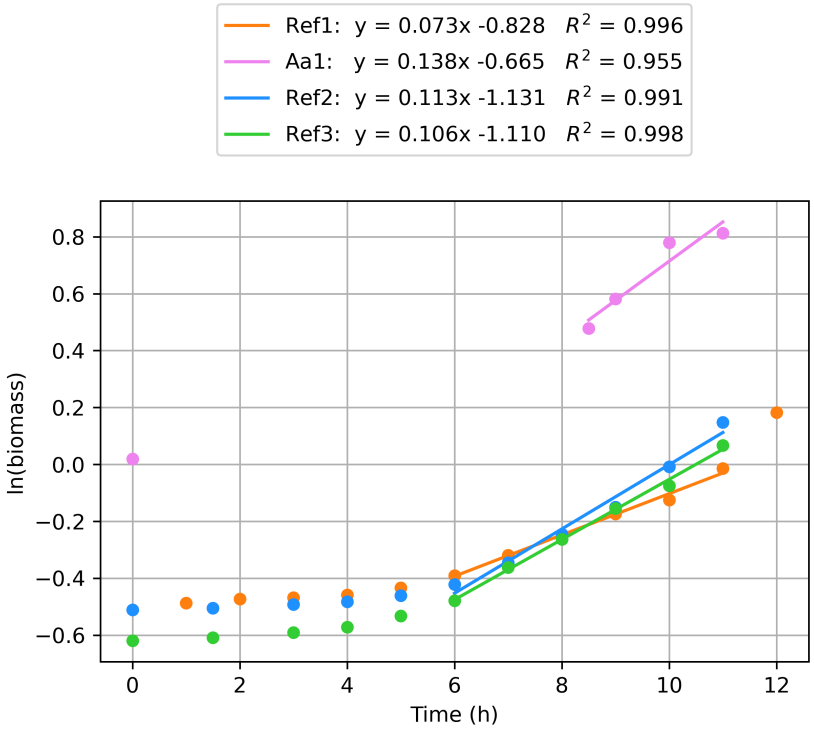

Figure H.2: Natural logarithm of biomass plotted against the time. The linear segments represent the exponential growth phases.

I

Gaseous oxygen balance method

The $k_L a$ can be determined with the gaseous oxygen balance method using Equation 18. Therefore, the values of the oxygen consumption, $F_{O_2}^{in} - F_{O_2}^{out}$, and the liquid oxygen concentration, c_l, during the fermentations are also valuable and are presented below.

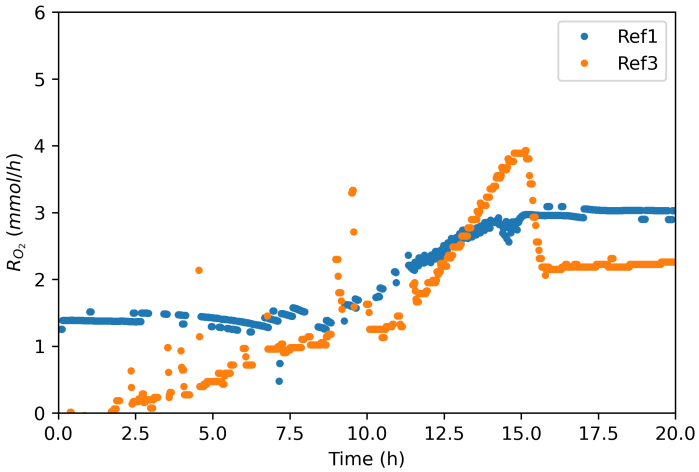

Figure I.1: Oxygen consumption throughout the fermentation process.

The oxygen consumption was determined as the difference between the oxygen in the inflowing and outflowing gas streams. At the start of the fermentation process, oxygen consumption is minimal. However, the graph from fermentation Ref1 begins above 1 mmol/h, suggesting the presence of a measurement error or an incorrect assumed parameter value. This could, for instance, originate from the oxygen concentration in the air, which was not measured on that date. The data from Ref3 looks more reliable, as it increases throughout the process and decreases suddenly, which indicated the end of the exponential growth phase.

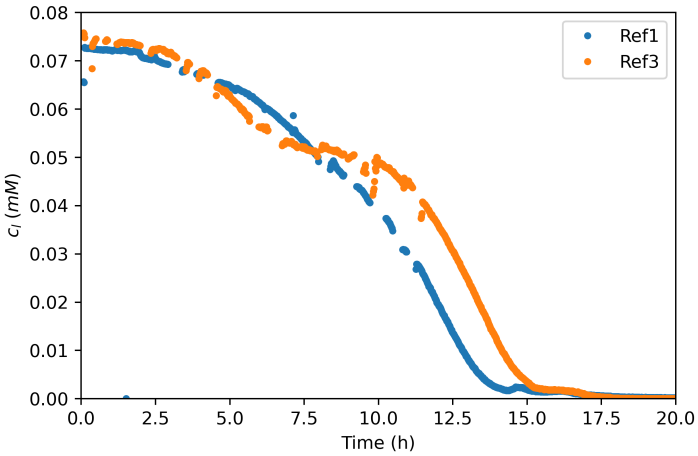

Figure I.2: Oxygen concentration in the liquid phase throughout the fermentation process.

As the consumption of oxygen increase throughout the fermentation, the oxygen mass transfer becomes insufficient to maintain the dissolved oxygen concentration, leading to its gradual decrease (Figure I.2).

J

Rheological models

The empirical correlations described in Section 1.2.7 account for the viscosity of the solution. During the rheology measurements, the rheometer records the applied shear stress (τ) and the resulting shear strain rate (γ) as data (Figure J.1). The shapes of these curves indicate that the rheological behavior of the samples is remains relatively constant throughout the fermentation process, with the exception of the sample collected after 6 hours.

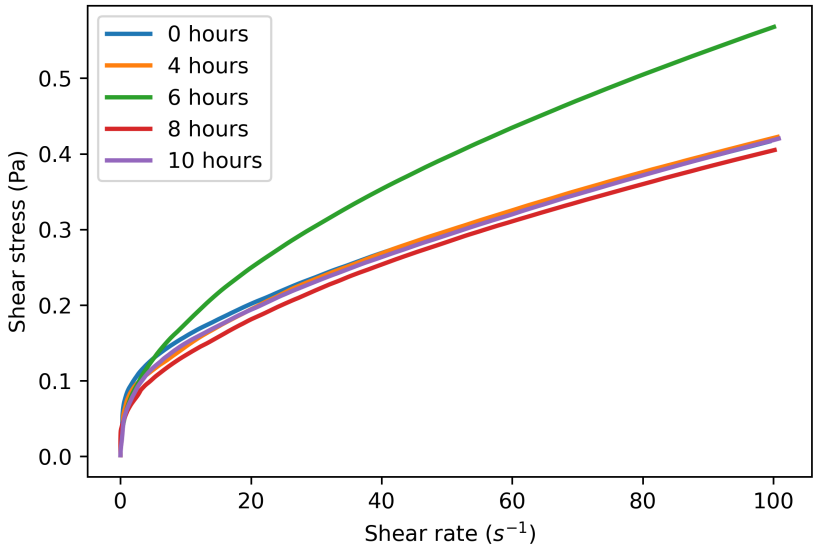

Figure J.1: Rheology measurements with samples from fermentation Ref3.

For Newtonian fluids, the viscosity is constant and can directly be calculated as the ratio of these parameters ($\mu = \tau / \gamma$). However, in non-Newtonian fluids, such as fermentation broths, viscosity varies with shear rate and must be described using rheological models. The empirical $k_L a$ correlations used to make prediction, indicate which rheological model must be used in combination with the empirical correlation. The different models are discussed below.

Ostwald-de Waele model / Power-law model

This model represent a relationship between the shear stress (τ) and the shear rate (γ), shown in Equation 28. The constant K is determined with the stirrer geometry and set at 11.5 (García-Ochoa and Gómez, 1998). The consistency index k ($Pa\ s^n$) and the flow behavior index n can be calculated by taking the logarithm (Equation 29) and plotting $\log(\tau)$ against $\log(\gamma)$. The slope will represent n and $\log(k)$ is the intersect of the graph, which were determined with linear regression. With these retrieved parameters, the effective viscosity can be determined with Equation 30. Perez and Sandall (1974) also used the power-law model but added a variation to determine the effective viscosity, shown in Equation 31.

$$\tau = k \cdot \gamma^n \tag{28}$$

$$\log(\tau) = n \cdot \log(\gamma) + \log(k) \tag{29}$$

$$\mu_{eff} = k \cdot (K \cdot N)^{n-1} \tag{30}$$

$$\mu_{eff} = k \cdot (K \cdot N)^{n-1} \cdot \left(\frac{3n+1}{4n}\right)^n \tag{31}$$

Figure J.2 shows that the region where the line is plotted effects the outcome of the values for k and n. Despite the optimization of linear regression, it was challenging to obtain reliable results with this method, resulting in some deviation between the obtained rheology values (Table 3.4).

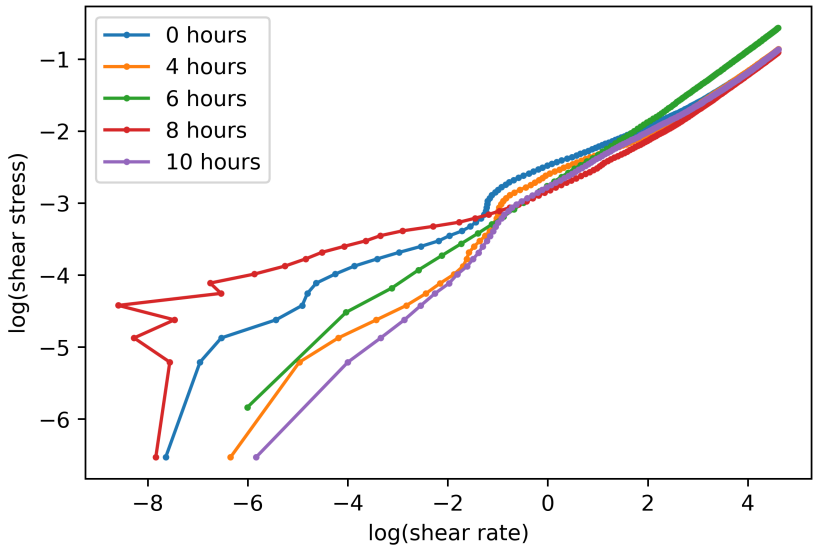

Figure J.2: Logarithmic values of rheological measurements of fermentation Ref3.

Casson model

With this rheological model, the relation between the shear stress (τ) and the shear rate (γ) is described using Equation 32. τ_0 is the yield stress (minimal stress required for the fluid to begin flowing) and k_c is the Casson consistency index, used to calculate the Casson viscosity (Equation 33). Plotting the square roots of the experimental data enables the determination of k_c, which is the slope. Figure J.3 suggest that the slopes should be similar, when excluding the sample after 6 hours. As can be seen in Table 3.4, the Casson viscosity's are relatively constant but still show a minor deviation. This could be attributed to the second power in Equation 33, enlarging the differences between the samples.

$$\sqrt{\tau} = \sqrt{\tau_0} + k_c \cdot \sqrt{\gamma} \tag{32}$$

$$\mu_c = k_c^2 \tag{33}$$

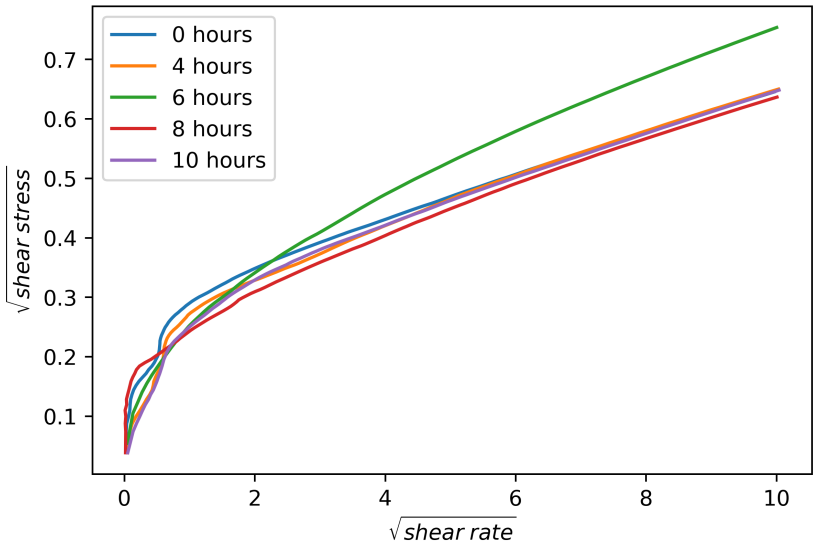

Figure J.3: Square root values of rheological measurements of fermentation Ref3.

K

Rheological properties Aa1 & Ref1

Only the values from fermentation Ref3 have been compared with prediction values. However, for fermentations Aa1 and Ref1, the viscosity was also measured, shown in Figure K.1.

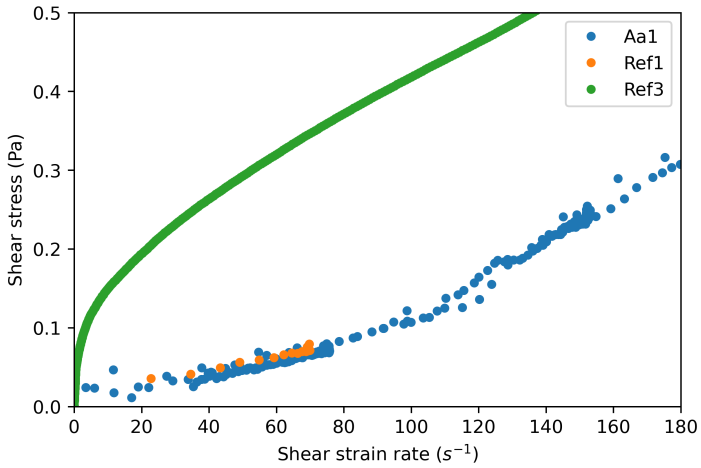

Figure K.1: Rheological results from different fermentations. For fermentations Ref1 and Ref3 the last sample is shown, for fermentation Aa1 the first sample. For Ref1, the shear rate was fixed at 0.1 Pa. For Aa1, the shear rate was fixed at 0.1 Pa, and at 0.2 Pa for a second measurement. In contrast, for Ref2, the applied shear ranged from 0 to 1 Pa, providing a more comprehensive rheological profile.

The data reveals significant differences in flow behavior. Fermentation Ref3 suggests shear-thinning behavior, whereas Ref1 and Aa1 seem to exhibit shear-thickening properties. This interpretation is supported by the flow behavior index values from Ref1, which exceed 1 (Table K.1), indicating shear thickening. However, according to literature, fermentation broths are typically shear-thinning (McNeil and Harvey, 1993, Newton et al., 2017). This discrepancy is likely due to the fact that samples from Ref1 and Aa1 were frozen and subsequently defrosted, as the rheometer was unavailable for some time. Freezing disrupts the cell membranes, releasing internal components into the broth, which can alter the rheological properties of the samples. As a result, the properties measured from Ref1 and Aa1 could not be reliably used for $k_L a$ prediction.

Property		**8 h**	**9 h**	**10 h**	**11 h**
Consistency Index	$k\ (Pa\ s^n)$	0.00018	0.00017	0.00012	0.00015
Flow Behavior Index	n	1.45	1.45	1.51	1.47
Effective Viscosity: Power-law	$\mu_{eff}\ (mPa\ s)$	1.25	1.21	1.10	1.16

Table K.1: Rheological properties from fermentation Ref1 at different time points.